VLASS Memo No. 26

VLASS Multi-Epoch Image Combination

Viral Parekh*, Juergen Ott, and James Khor
NRAO, Socorro

April 2026

Abstract

In this memo, we investigate the multi-epoch image combination of the VLA Sky Survey (VLASS) Quick Look (QL) and Single Epoch (SE) maps. Since VLASS images, from different epochs, can have different restoring beams and spatially varying noise properties, direct image combination is not straightforward. To address this, all input maps are first regridded to a common pixel grid and smoothed to a common beam. The images are then combined using local RMS-based inverse-variance weighting to produce weighted-mean and weighted-median stacked maps. The local RMS weighted mean allows noisier regions and noisier epochs to be downweighted, improving the sensitivity to persistent faint emission while reducing the influence of residual imaging artifacts and localized background variations. The weighted median provides an additional robust product against outliers in individual epochs. This analysis suggests that the combined images provide improved noise performance and dynamic range relative to the individual epoch maps. To preserve the total flux densities of radio sources, we convert all input maps to Kelvin (K) from Jy beam^{-1}, before convolution. After convolving to the common beam, we convert them back to Jy beam^{-1} unit. Flux comparisons using total, peak, and island measurements show that the combined maps generally reduce part of the scatter present between individual epochs and are often closer to the later VLASS epochs than to the earlier ones. In particular, island total-flux ratios are usually greater than unity for both QL and SE combined products, indicating that the combined maps tend to recover slightly more island-scale emission than the individual epoch maps, consistent with their improved sensitivity. The SE maps show better overall agreement with their combined products than the QL maps, likely because the self-calibrated SE images provide more stable flux recovery and improved image fidelity. We also developed and are currently testing a Flask-based VLASS cutout server as a practical platform for visualization and image-combination experiments.

1 Introduction

In astronomy, image combination and stacking are widely used to enhance sensitivity to faint emission and to suppress random noise. When multiple independent astronomical images

*vparekh@nrao.edu

are combined, the noise in the final stacked image decreases approximately as $1/\sqrt{N}$, where N is the number of input images, provided that the noise between images is uncorrelated. This makes stacking a powerful technique for recovering low-surface-brightness emission that may not be visible in any single image. In radio interferometric observations, however, image combination is not straightforward because the angular resolution of an image depends on both the baseline distribution of the array and the observed frequencies within the band. The effective point-spread function of an interferometric image, usually described by the restoring beam, is generally represented by an elliptical Gaussian characterized by its major axis (Bmaj), minor axis (Bmin), and position angle (PA). The exact beam shape and size can vary between observations because of differences in uv coverage, frequency setup, array configuration, weighting scheme, and the amount of flagged data from individual antennas, baselines, or channels. As a result, images of the same source obtained in different epochs often have different beam sizes and orientations. These differences can significantly affect the apparent morphology and peak brightness of a source, making direct pixel-by-pixel comparison or stacking unreliable unless the beam mismatch is first corrected. Therefore, before combining multi-epoch radio images, it is necessary to homogenize them to a common beam so that all images represent the sky at the same effective angular resolution. Only after this step can the images be meaningfully combined to improve sensitivity while preserving a consistent interpretation of source structure and flux distribution.

2 VLASS data

The VLA Sky Survey (VLASS) is an S-band (2–4 GHz), B-configuration survey carried out with the Karl G. Jansky Very Large Array, covering the sky north of $\delta = -40^\circ$ (Lacy et al., 2020). The final observing campaign, VLASS4.1, ran from September 2025 to February 2026 and will replace the earlier VLASS1.1 observations in the final Single Epoch (SE) and cumulative image products for half of the survey area. Quick Look (QL) images are available for the first three VLASS epochs, and QL image production for VLASS4.1 is ongoing. Typically, JVLA B-configuration ($\sim$ 11 km) with S-band provides resolution $\theta_{\rm HPBW} \approx 2$ arcsec. VLASS multi-epoch images have different beam sizes and position angles, so it is not straightforward to stack these images without taking care of their beams. This is necessary because the synthesized beam varies slightly between epochs in size and orientation, and such differences would otherwise affect flux distribution and source morphology in the combined image.

3 Beam convolution

In order to match the common beam across all epochs of VLASS images, we used the `radio-beam` package[1] to compute the common beam, defined as the smallest Gaussian beam to which all input beams can be validly convolved. Rather than averaging beam parameters or selecting the largest beam dimensions independently, `radio-beam` solves the full two-dimensional beam-matching problem using the geometry of elliptical Gaussian. For two beams, it applies an exact analytic solution adapted from CASA (`ia.commonbeam` which determines a beam to which all beams in an image can be convolved). For larger beam sets, it samples the edges of all beam ellipses, constructs their convex hull, and uses the Khachiyan algorithm to find the minimum-volume ellipse enclosing the full set (Fig. 1). Because this enclosing-ellipse method is approximate, the package applies a very small correction factor to avoid underestimating the true enclosing beam, and if necessary, it increases that factor until the resulting solution can be deconvolved from every input beam. The final common

[1] https://github.com/radio-astro-tools/radio-beam

beam is then used as the target resolution, and each epoch image is convolved to that beam prior to producing stacked maps, ensuring that the final VLASS image combinations are compared and combined at the matched angular resolution. In our beam convolution procedure, we used CASA's `imsmooth` task to convolve the input VLASS images. Before image convolution, we regridded each input image to the corresponding VLASS epoch 2 to align the WCS coordinates and pixel sizes across all epoch images. We selected VLASS epoch 2, as it is the middle epoch. For regridding, we used CASA's `imregrid` task.

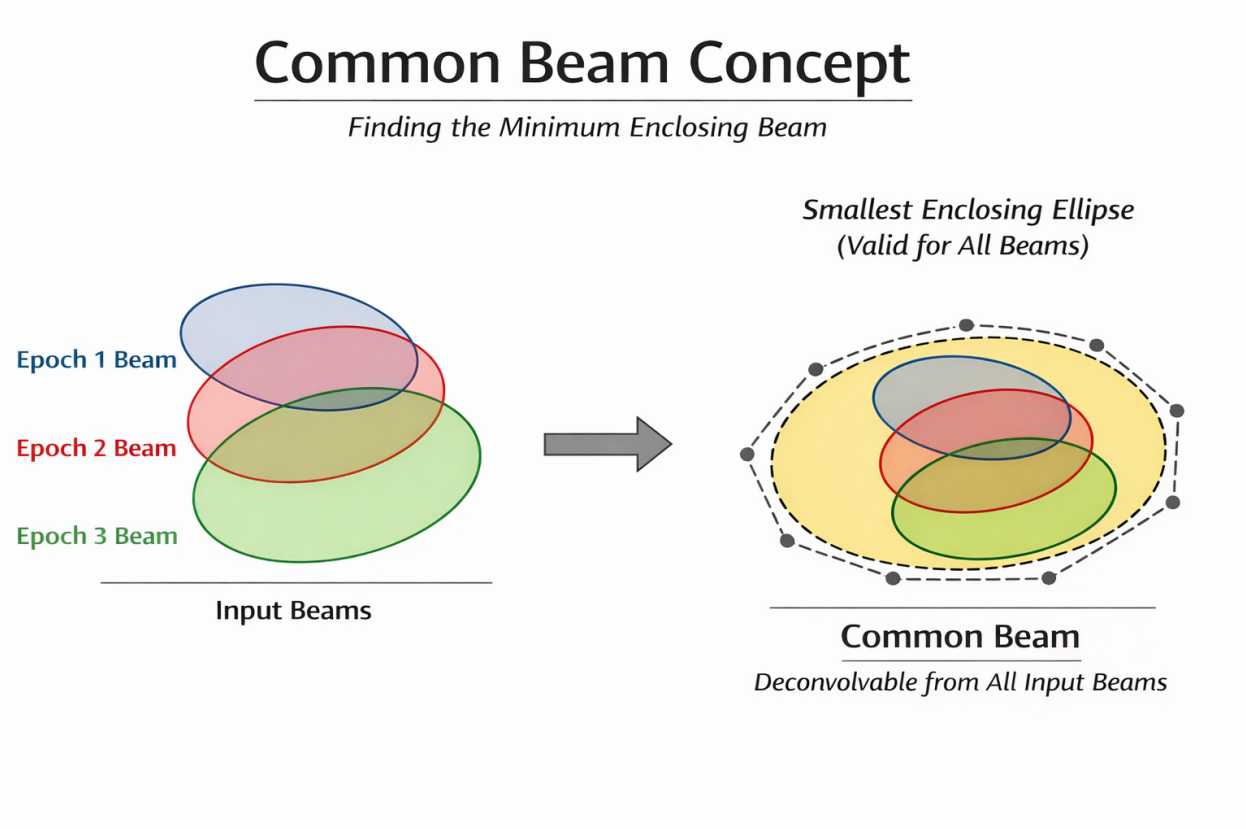

Figure 1: Schematic diagram of common-beam approach.

3.1 Jy beam^{-1} to K conversion for beam-matched stacking

Because the VLASS multi-epoch images have different restoring beams, we convert the images from Jy beam^{-1} to brightness temperature (K) before convolution to a common beam. This is necessary because Jy beam^{-1}, depends on the beam area, so the same sky surface brightness can correspond to different numerical values if the beam sizes differ. Brightness temperature, by contrast, provides a beam-normalized measure of surface brightness and is therefore more suitable for comparing and smoothing images with different angular resolutions.

The conversion from flux density (Jy) per beam to brightness temperature is

$$T_{\rm B} = \frac{S_\nu\, c^2}{2k_{\rm B}\, \nu^2\, \Omega_{\rm beam}},$$

with beam solid angle

$$\Omega_{\rm beam} = \frac{\pi}{4\ln 2}\, \theta_{\rm maj}\, \theta_{\rm min},$$

where $\theta_{\rm maj}$ and $\theta_{\rm min}$ are the FWHM beam axes in radians. In practical units, this becomes

$$T_{\rm B}[{\rm K}] \approx 1.222 \times 10^6\, \frac{S_\nu[{\rm Jy\,beam^{-1}}]}{\nu^2_{\rm GHz}\, \theta_{\rm maj}['']\, \theta_{\rm min}['']}.$$

After conversion to K, the images are convolved to the target common beam and then stacked. If needed, the final convolved image is converted back to Jy beam^{-1} using the target beam:

$$S_\nu[\mathrm{Jy\,beam^{-1}}] \approx \frac{T_\mathrm{B}[\mathrm{K}]\,\nu^2_\mathrm{GHz}\,\theta_\mathrm{maj}[''']\,\theta_\mathrm{min}[''']}{1.222\times10^6}.$$

This final conversion is useful because Jy beam^{-1} is the standard unit for most interferometric image products and is easier to interpret in terms of peak flux density and comparison with survey images or catalogs. In this our image combination process, we convert back each VLASS image to the Jy beam^{-1} unit.

4 Image stacking - RMS-weighted mean and median maps

After beam homogenization (and regridding), the images are combined using local RMS-based inverse-variance weighting. Let $I_k(x, y)$ denote the image value at pixel (x, y) in the kth epoch, where $k = 1, \ldots, N$. For each epoch image, we estimate a local RMS map, $\sigma_k(x, y)$, using a running window W centered on each pixel. The local RMS is calculated from the first and second moments of the image values within the window,

$$\sigma_k(x,y) = \sqrt{\langle I_k^2\rangle_W - \langle I_k\rangle_W^2},$$

where $\langle I_k\rangle_W$ is the local mean of the image values inside the window and $\langle I_k^2\rangle_W$ is the local mean of the squared values. This expression is simply the local standard deviation, evaluated in a moving box across the image. In this way, each epoch is assigned a spatially varying noise map rather than a single global RMS value.

From the local RMS map, a weight map is defined as

$$w_k(x,y) = \frac{1}{\sigma_k^2(x,y)}.$$

This is the standard inverse-variance weighting scheme. Pixels with lower local RMS receive larger weights, while pixels with higher local RMS receive smaller weights. Therefore, regions with lower local RMS contribute more strongly to the final stacked image, whereas regions with higher local RMS receive less weight automatically.

The RMS-weighted mean stacked image is then computed as

$$I_\mathrm{stack}(x,y) = \frac{\sum_{k=1}^N w_k(x,y)\,I_k(x,y)}{\sum_{k=1}^N w_k(x,y)}.$$

This equation gives the weighted average of the input images at each pixel. The numerator is the sum of the weighted pixel values from all epochs, and the denominator is the sum of the weights. If the local noise is approximately Gaussian and uncorrelated between epochs, this inverse-variance weighted mean gives an efficient estimate of the true sky brightness at that position.

In addition to the weighted mean, we also construct a weighted median stack. For each pixel (x, y), the set of values $\{I_k(x, y)\}$ from all epochs is sorted in increasing order. The corresponding weights $\{w_k(x, y)\}$ are arranged in the same order, and the cumulative weight is then computed. The weighted median is defined as the first sorted value for which the cumulative weight reaches or exceeds one-half of the total weight. In this way, the weighted median also takes into account the local RMS information, but is less sensitive than the weighted mean to extreme outliers in individual epochs.

The use of local RMS-based weighting is particularly useful for multi-epoch VLASS data, because the noise properties are not uniform either within a single image or between different epochs. The local RMS can vary because of residual sidelobes around bright sources, imperfect deconvolution, calibration errors, changes in flagged data fraction, variable uv coverage, and spatial changes in the background noise. If a single global RMS value were used for each epoch, these local differences would be ignored, and noisy image regions could contribute too strongly to the final combined image. By constructing a local RMS map for every epoch, the stacking procedure can respond to the actual noise level at each position in the image.

This procedure improves the signal-to-noise ratio of persistent sky emission in the final stacked product. Emission that is present in multiple epochs add coherently, while random noise decreases through averaging. Because the weights are higher in lower-noise regions, the final stack is more strongly influenced by the best-quality measurements. This improves the sensitivity to faint sources and low-surface-brightness emission that may be below the detection threshold in the individual epoch images. In addition, the weighted median provides a more robust stacked product in the presence of occasional bad pixels, residual imaging artifacts, or localized outliers. VLASS memo 22 also explained about median stacking technique for QL maps.

5 Local cutout server

5.1 Flask-based cutout server

To interactively inspect and combine VLASS images, we developed a lightweight cutout server using the `Flask` Python web framework. This is a complementary cutout server along with other existing (e.g., CIRADA), to test and study mainly the image combination process for a given target position and size of the cutouts. The server acts as a front-end interface between the user, the VLASS archive products, and the external CASA-based stacking pipeline. Given either an object name or sky coordinates, the server can perform optional SIMBAD/NED name resolution, identify the relevant VLASS tiles, download the corresponding FITS images from the NRAO quicklook and single-epoch data repositories, and generate sky cutouts centered on the requested target (Fig. 2 is the web interface page). The user can select the cutout size in pixels or angular size around the target. The user can also supply the RMS window size (in pixels) to generate the RMS map. We found that a box size of 10-20 would give reasonable RMS maps for VLASS data. The current implementation supports both QL images and SE self-calibrated maps, and also include the mean and median QL/SE stack products when available multi epoch images. For each retrieved epoch, the server prepares display products and downloadable files, including the FITS cutout itself, a rendered PNG preview, and summary metadata such as beam size and RMS. The Flask application does not perform the image regridding, beam matching, or stacking internally; instead, it passes the cutout FITS files to an external CASA script, which carries out the regridding, common-beam smoothing, local-RMS estimation, and the production of inverse-variance weighted mean and weighted-median stacked maps. The resulting stacked FITS files and preview images are then returned to the web interface and displayed alongside the individual epoch cutouts. To keep the workflow lightweight, the server uses temporary working directories during processing, serves generated downloads directly from memory, and removes intermediate FITS files from disk after completion. In this way, the Flask cutout server provides a simple browser-based environment for querying VLASS data, visualizing multi-epoch maps, inspecting beam and noise properties, and interactively generating stacked image products for a selected target.

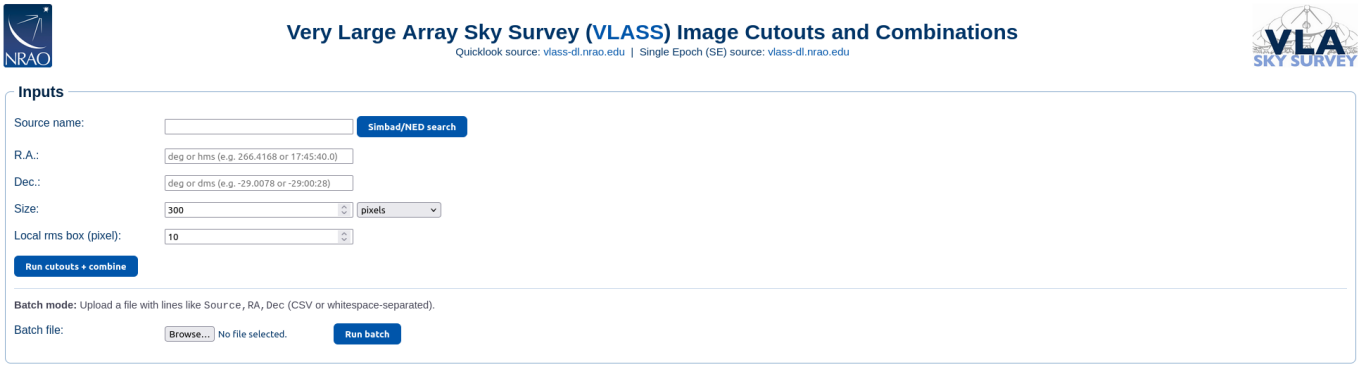

Figure 2: VLASS cutout server. User can search for the object name with a Simbad/NED query or directly enter the RA and Dec of the object. The user can select the cutout size in pixels or angular size. The user can also select the RMS box size to calculate the local noise and generate an RMS map. The cutout server can also take a batch file to search and display images of more than one object..

6 Results

6.1 VLASS cutouts

We searched and downloaded the VLASS QL and SE cutout maps for the position RA = 2:42:08.1000 and the Dec = -1:28:35.601 with a size of 600 pixels, using our cutout server. The resulting cutout images are shown in Figures 3 and 4 with the corresponding stacked images. To generate RMS maps, we used a window box size of 10 pixels. For QL maps, we found all four epoch maps, and for SE, we found epoch 2 and 3 images in the archive. We combined these respective maps after regridding and common-beam convolution and displayed the RMS weighted mean and median maps in Figures 3 and 4. For SE maps, we only generated the mean map from only two epoch data. We also listed beam sizes, RMS and dynamic ranges (DR) for each of the images in Tables 1 and 2 for QL and SE maps, respectively. In these tables, we also list the RMS ratios between the single epoch and combined map to compare the improvements in stacked images.

Table 1: VLASS QL cutout maps beam sizes (original) and RMS values. We convolved each individual VLASS epoch map to a common beam to generate combined mean and median maps. The RMS ratio column gives the ratio of the RMS in each map relative to the RMS-weighted mean and RMS-weighted median maps, respectively. The last column is dynamic range which is Peak flux /RMS.

VLASS QL maps	Beam sizes (Bmin, Bmaj, PA)	RMS (mJy beam^{-1})	RMS ratio (to mean/to median)	DR
VLASS 1	$3.948'' \times 2.214''$, 42.48°	0.140	1.57/1.25	114
VLASS 2	$3.231'' \times 2.190''$, 29.69°	0.188	2.11/1.68	74
VLASS 3	$2.771'' \times 2.224''$, 16.23°	0.165	1.85/1.47	90
VLASS 4	$2.889'' \times 1.935''$, -4.71°	0.141	1.58/1.26	85
RMS-weighted mean	$4.014'' \times 2.540''$, 37.96°	0.089		202
RMS-weighted median	$4.014'' \times 2.540''$, 37.96°	0.112		160

6.2 VLASS full maps

In order to compare source fluxes and rms after image combination, we downloaded the archival QL and SE maps of default size 1° (VLASS Tile T08t02 and Source id J004201-

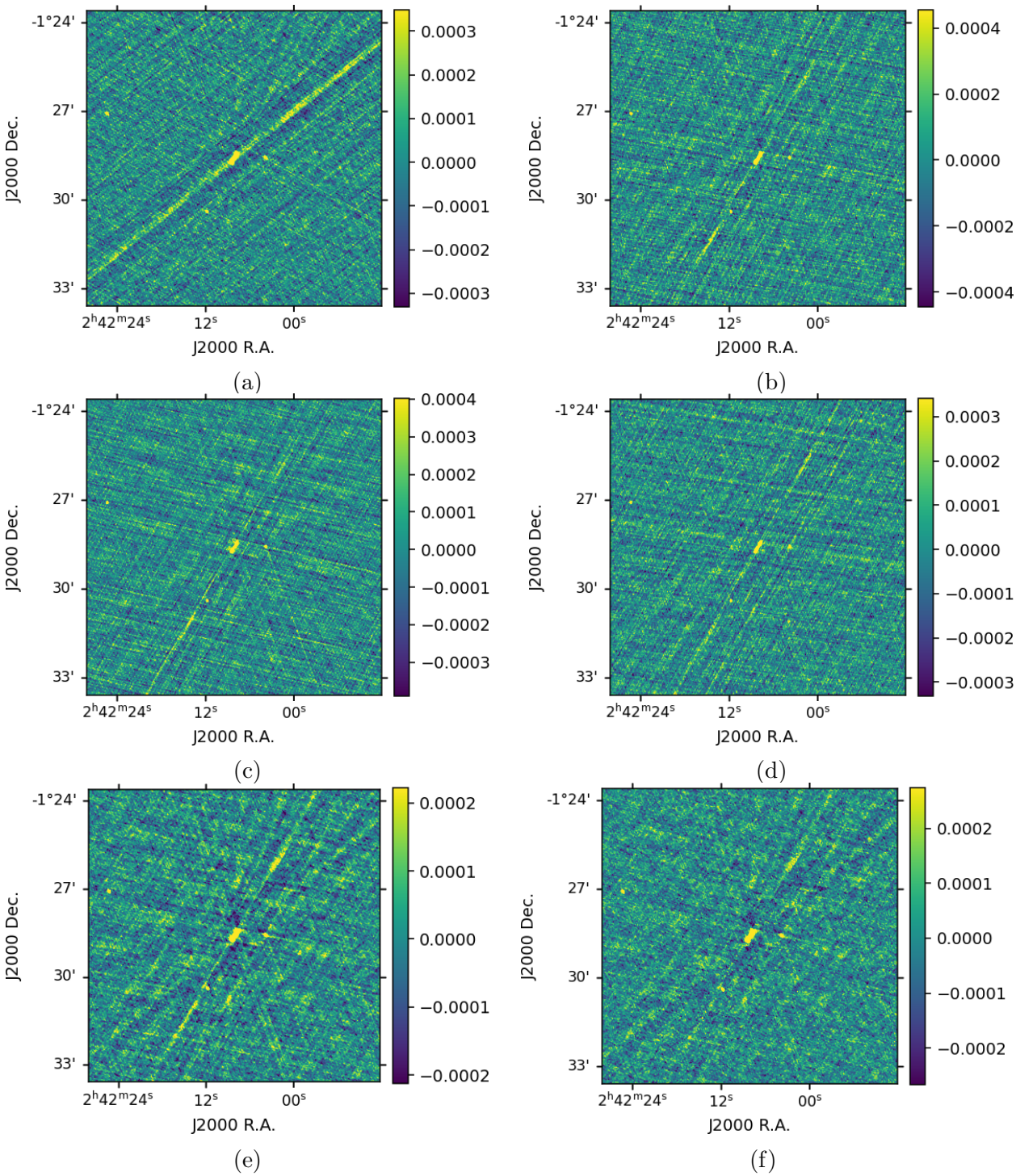

Figure 3: VLASS QL cutout maps for four VLASS epochs. (a) VLASS1, (b) VLASS2, (c) VLASS3, (d) VLASS4, (e) RMS-weighted mean map, and (f) RMS-weighted median map. Images (e) and (f) are convolved with the common beam and after stacking all four epoch maps. The unit of colorbar is Jy/b.

Table 2: VLASS cutout SE maps beam sizes (original) and RMS values. We convolved each individual VLASS SE epoch map to a common beam to generate a combined mean map.

VLASS SE maps	Beam sizes (Bmin, Bmaj, PA)	RMS (mJy beam^{-1})	RMS ratio (to mean)	DR
VLASS 2	$3.212'' \times 2.208''$, 28.30°	0.166	1.44	90
VLASS 3	$2.759'' \times 2.207''$, 15.00°	0.155	1.35	96
RMS-weighted mean	$3.227'' \times 2.271''$, 27.31°	0.115		147

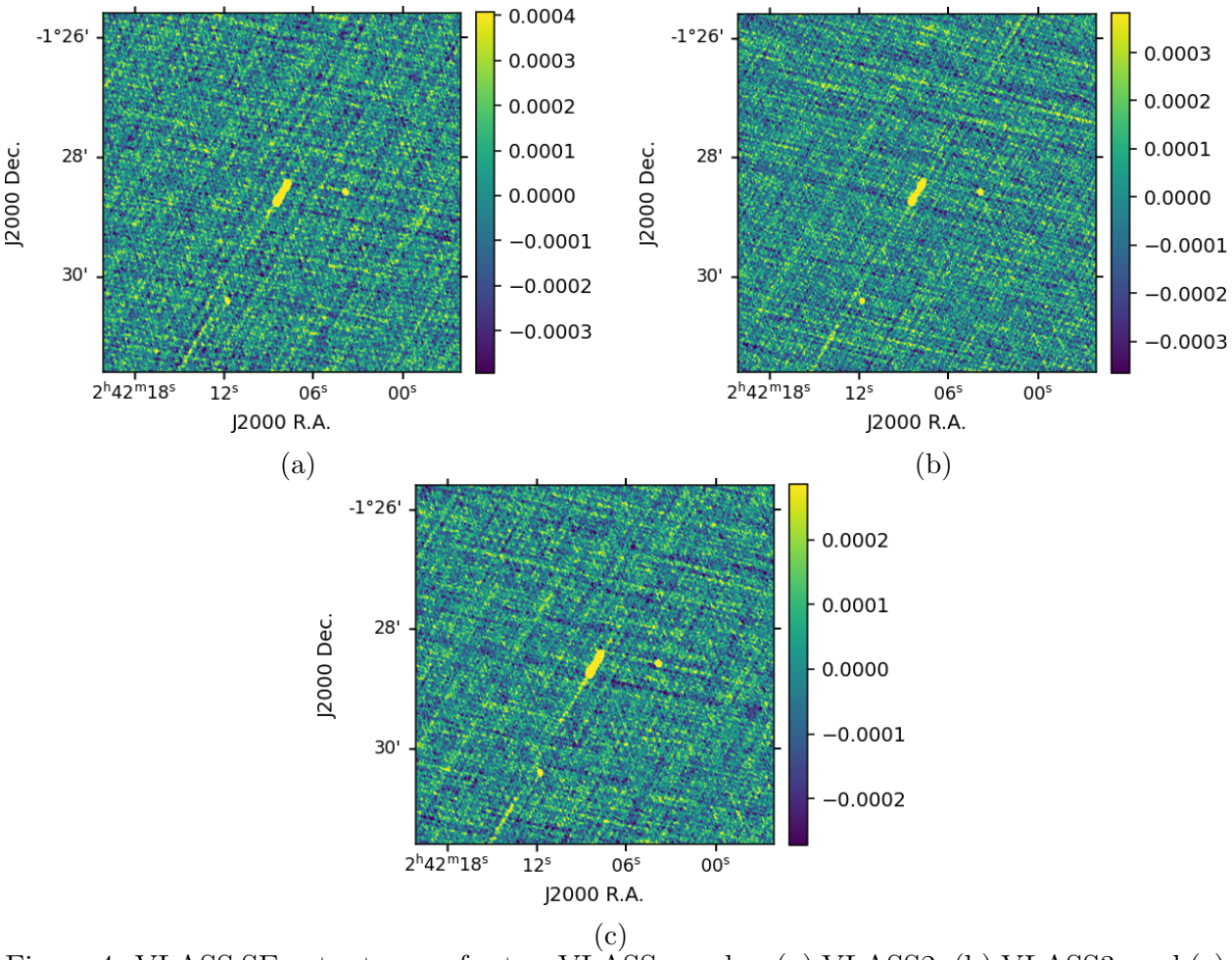

Figure 4: VLASS SE cutout maps for two VLASS epochs. (a) VLASS2, (b) VLASS3, and (c) RMS-weighted mean map.Image (c) is convolved with the common-beam and after stacking two epoch maps. The unit of colorbar is Jy/b.

093000). In the archive, for QL, we found maps for VLASS epoch 1 (1.2), 2 (2.2), 3 (3.2), and 4 (4.2), and for SE, we found maps for VLASS epoch 2 (2.2) and 3 (3.2). Then, as mentioned above for both QL and SE maps, we used VLASS 2 as the template image and regridded other epoch maps to it, followed by convolving each map to the common beam for a set of QL and SE maps. We convolved all QL maps to the beam size of $3.78'' \times 2.32''$, 20.48° and SE maps to $3.23'' \times 2.27''$, 15.89°. Then we combined these two sets of maps and generated RMS weighted mean and median maps. Since for SE maps, only epochs 2 and 3 were available, we generated an RMS weighted mean map. We show QL and its combined maps in Figs. from 5 to 10, and SE and its combined mean map in Figs. from 11 to 13. We listed RMS and dynamic range values for QL and SE maps in Tables 3 and 4, respectively.

We used the PyBDSF to extract the total flux densities, peak and island fluxes[2] of radio sources in all of these maps. To cross-match sources among these maps, we used a tolerance radius of $1''$. We compared the individual epoch of the VLASS map with the weighted mean and weighted median combined maps using total flux, island total flux, and peak flux values. We focus here on two simple measures: the median ratio and the mean percentage difference. A median ratio close to 1 means the combined map agrees well with the single-epoch map. Values below 1 mean the combined map is slightly fainter, while values above 1 mean it is slightly brighter. In all flux density calculations, we included quadrature uncertainties (see

[2]In PyBDSF, the island flux is the total integrated flux measured over a contiguous region of connected pixels above the detection threshold, representing the full emission area associated with a potential source or group of blended sources.

Appendix). Below, we will show comparisons for each of the QL and SE maps.

6.2.1 VLASS QL maps

For QL maps flux comparison (of single epoch) with combined mean and median maps, we found for total flux, the combined maps matched VLASS3 and VLASS4 better than VLASS1 and VLASS2. The mean percentage differences were 10.77% and 8.42% for VLASS1, 9.33% and 8.40% for VLASS2, 6.61% and 6.18% for VLASS3, and 6.67% and 6.72% for VLASS4, for the weighted mean and weighted median maps, respectively. The median ratios were slightly below 1 for all epochs, showing that the combined maps usually recover slightly lower total flux than the individual epoch maps. The closest agreement was seen for VLASS4, with median ratios of 0.980 for the weighted mean map and 0.991 for the weighted median map. VLASS3 also showed small mean percentage differences, indicating that the combined maps are most similar to the later epochs in total flux.

For the island total flux, the best agreement was again found for VLASS3 and VLASS4, while VLASS2 showed the largest discrepancy. The mean percentage differences were 8.18% and 4.86% for VLASS1, 27.50% and 22.63% for VLASS2, 4.85% and 4.93% for VLASS3, and 4.21% and 5.35% for VLASS4, for the weighted mean and weighted median maps, respectively. The median ratios were close to 1 in most cases, especially for VLASS3, where the weighted median map gave a value of 1.003. Unlike total flux, the island-flux ratios were usually slightly above 1, suggesting that the combined maps tend to recover a little more island-scale emission than the single-epoch maps. The much larger differences for VLASS2 suggest that the extended or blended emission in that epoch is less consistent with the stacked products.

For the peak flux, the closest agreement was seen for VLASS2 and VLASS4, while VLASS3 showed the largest difference. The mean percentage differences were 2.65% and 2.15% for VLASS1, 1.06% and 1.12% for VLASS2, 3.91% and 5.22% for VLASS3, and 1.91% and 1.94% for VLASS4, for the weighted mean and weighted median maps, respectively. The median ratios support the same trend. VLASS4 was especially well matched, with ratios of 1.018 for the weighted mean map and 0.996 for the weighted median map, while VLASS2 also showed close agreement. In contrast, VLASS3 had noticeably lower ratios of 0.887 and 0.874, showing that the combined maps have lower peak brightness than that epoch, even though the total flux agreement is fairly good.

Taken together, these comparisons show that the combined maps are generally closer to the later epochs than to the earlier ones. For total flux and island total flux, the best agreement is with VLASS3 and VLASS4. For peak flux, the closest match is with VLASS2 and VLASS4. VLASS4 is the most consistently similar to the combined maps, especially in terms of median ratio, while VLASS2 stands out as the most discrepant in island total flux and VLASS3 differs the most in peak flux. We plotted total, peak, and island fluxes for VLASS QL individual epoch vs combined mean and median maps from Figs. 14 to 37. We listed all statistical values for QL maps in the Appendix Table 5.

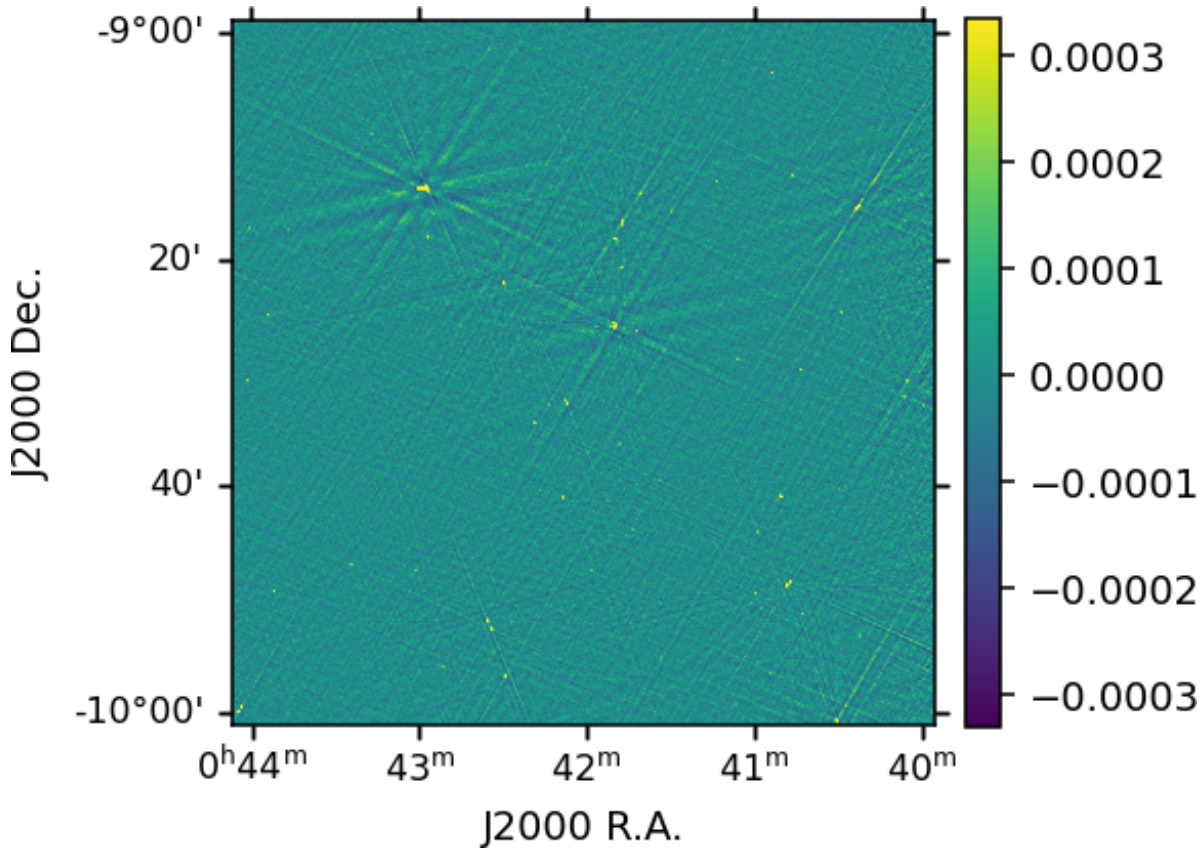

Figure 5: VLASS1 QL map. The image is convolved with a common beam of $3.78'' \times 2.32''$, PA $= 20.48°$. The unit of the colorbar is Jy beam^{-1}.

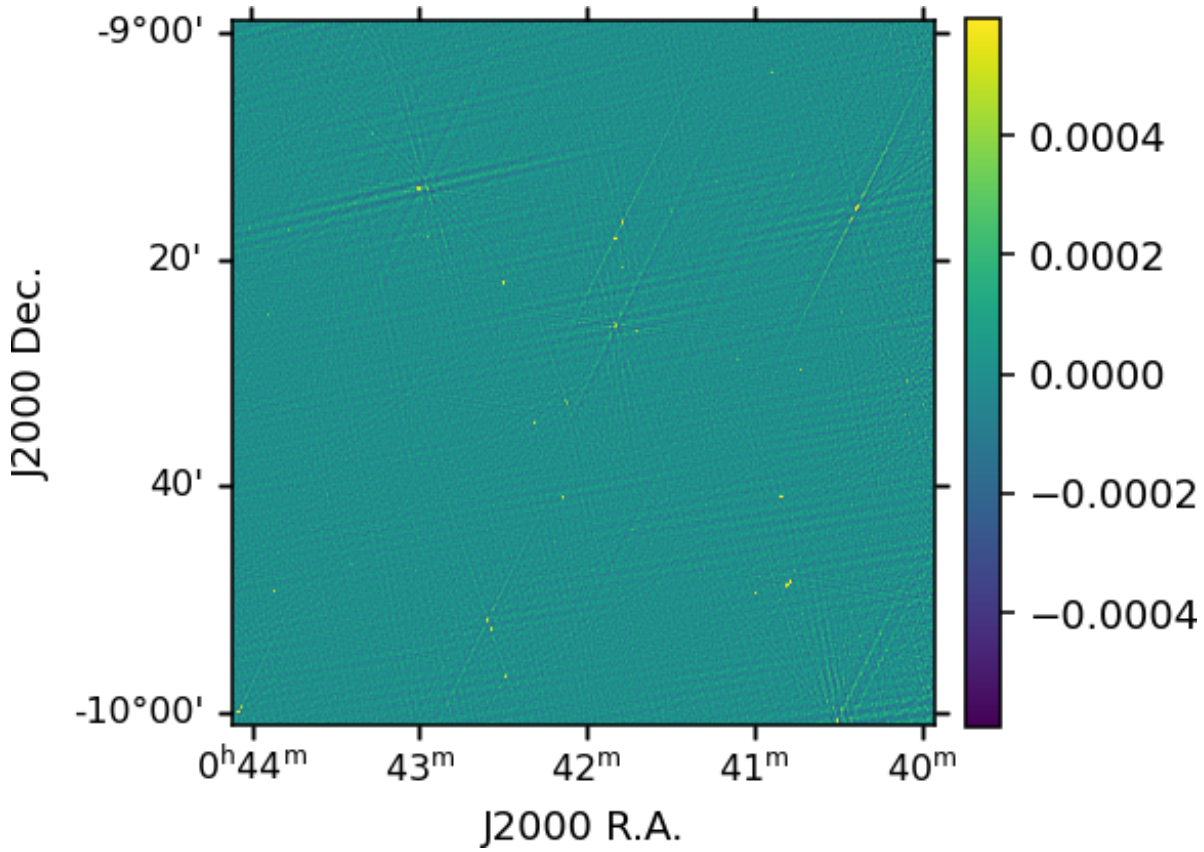

Figure 6: VLASS2 QL map. The image is convolved with a common beam of $3.78'' \times 2.32''$, PA $= 20.48°$. The unit of the colorbar is Jy beam^{-1}.

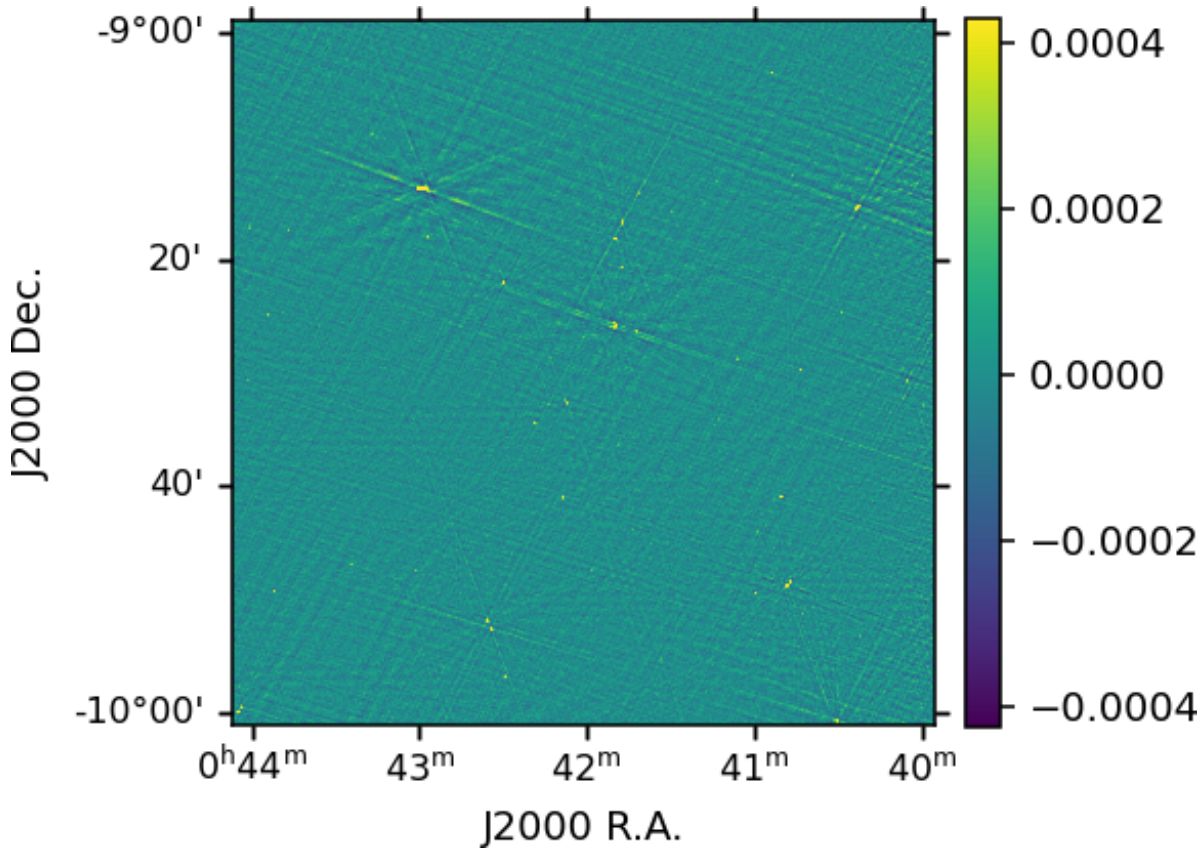

Figure 7: VLASS3 QL map. The image is convolved with a common beam of $3.78'' \times 2.32''$, PA $= 20.48°$. The unit of the colorbar is Jy beam^{-1}.

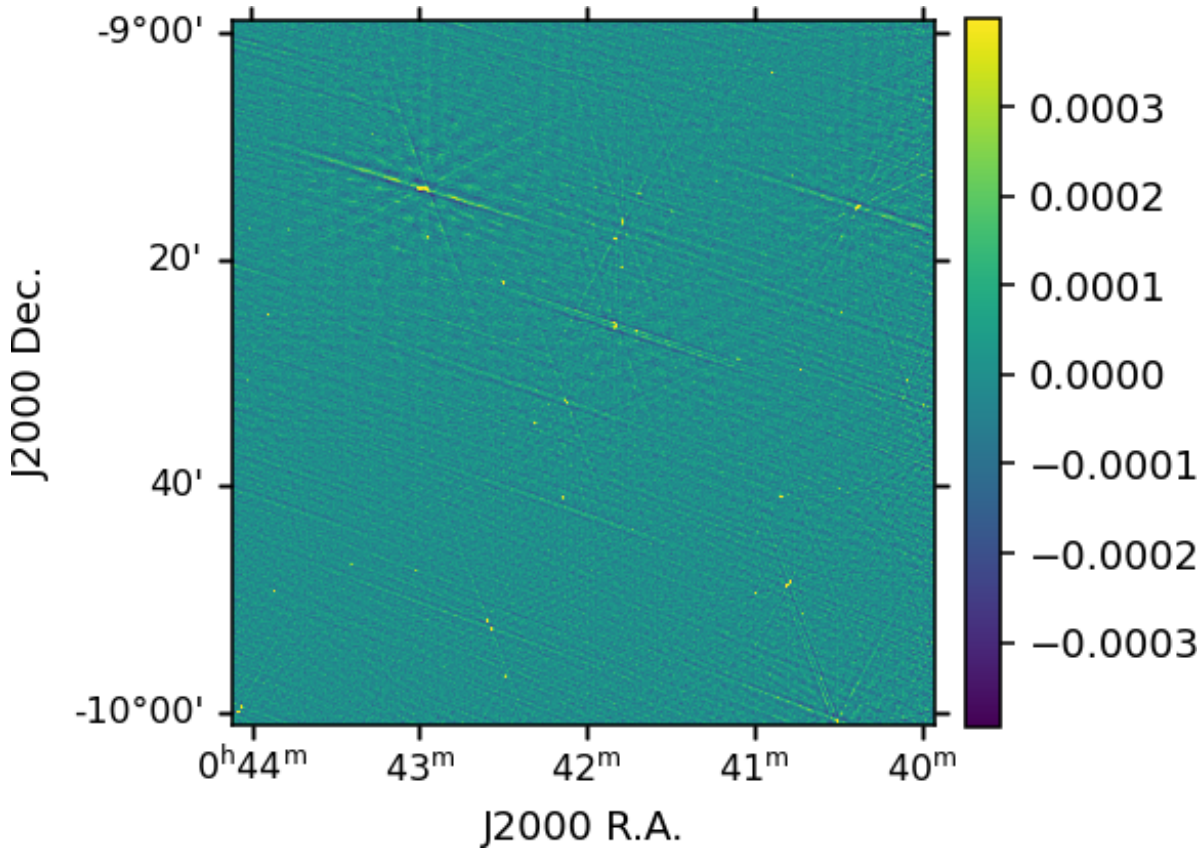

Figure 8: VLASS4 QL map. The image is convolved with a common beam of $3.78'' \times 2.32''$, PA $= 20.48°$. The unit of the colorbar is Jy beam^{-1}.

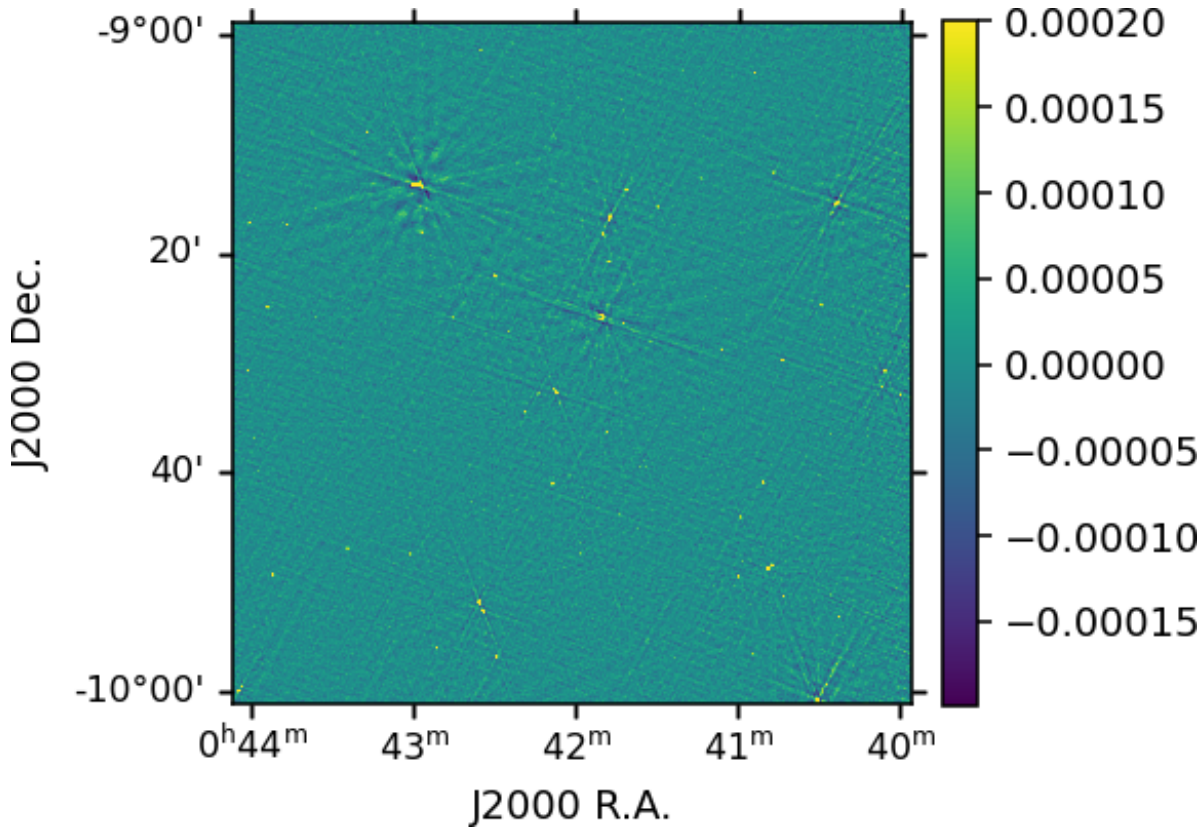

Figure 9: RMS-weighted mean QL map. The image is convolved with a common beam of $3.78'' \times 2.32''$, PA $= 20.48°$. The unit of the colorbar is Jy beam^{-1}.

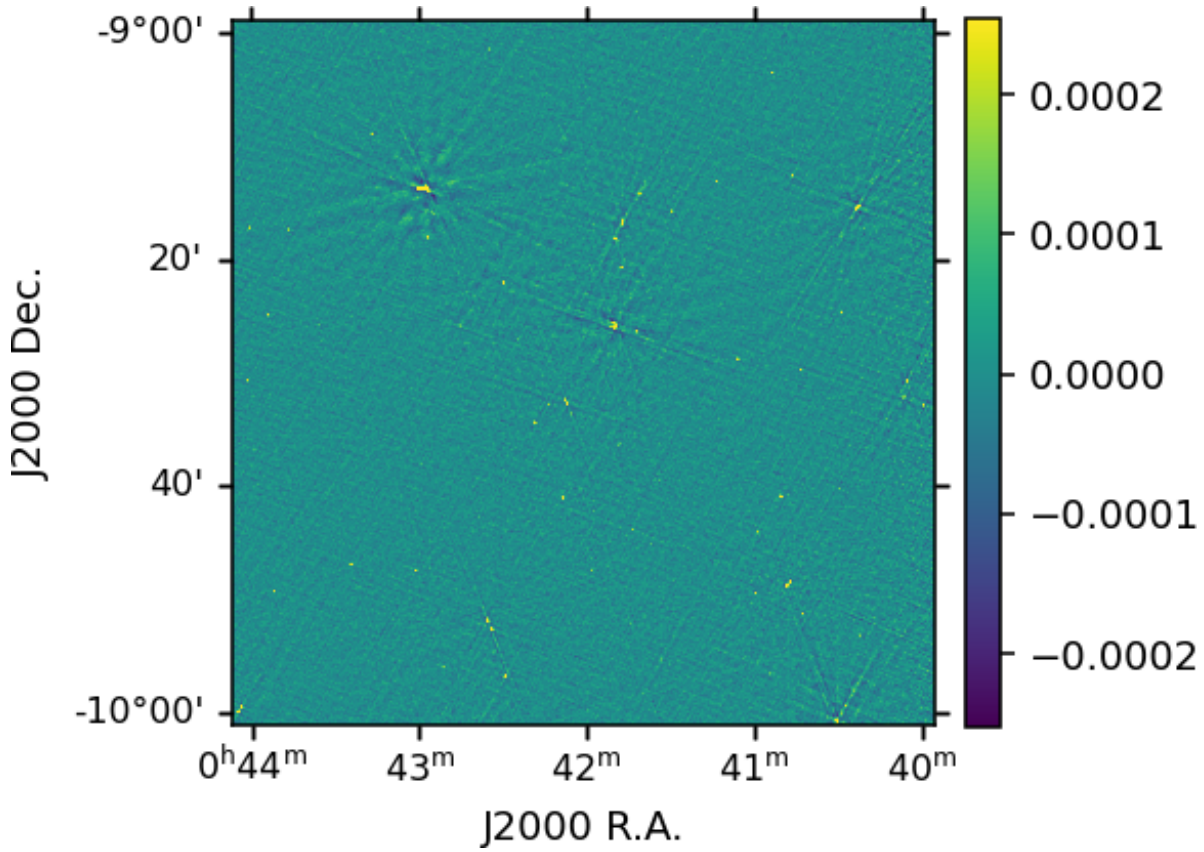

Figure 10: RMS-weighted median QL map. The image is convolved with a common beam of $3.78'' \times 2.32''$, PA $= 20.48°$. The unit of the colorbar is Jy beam^{-1}.

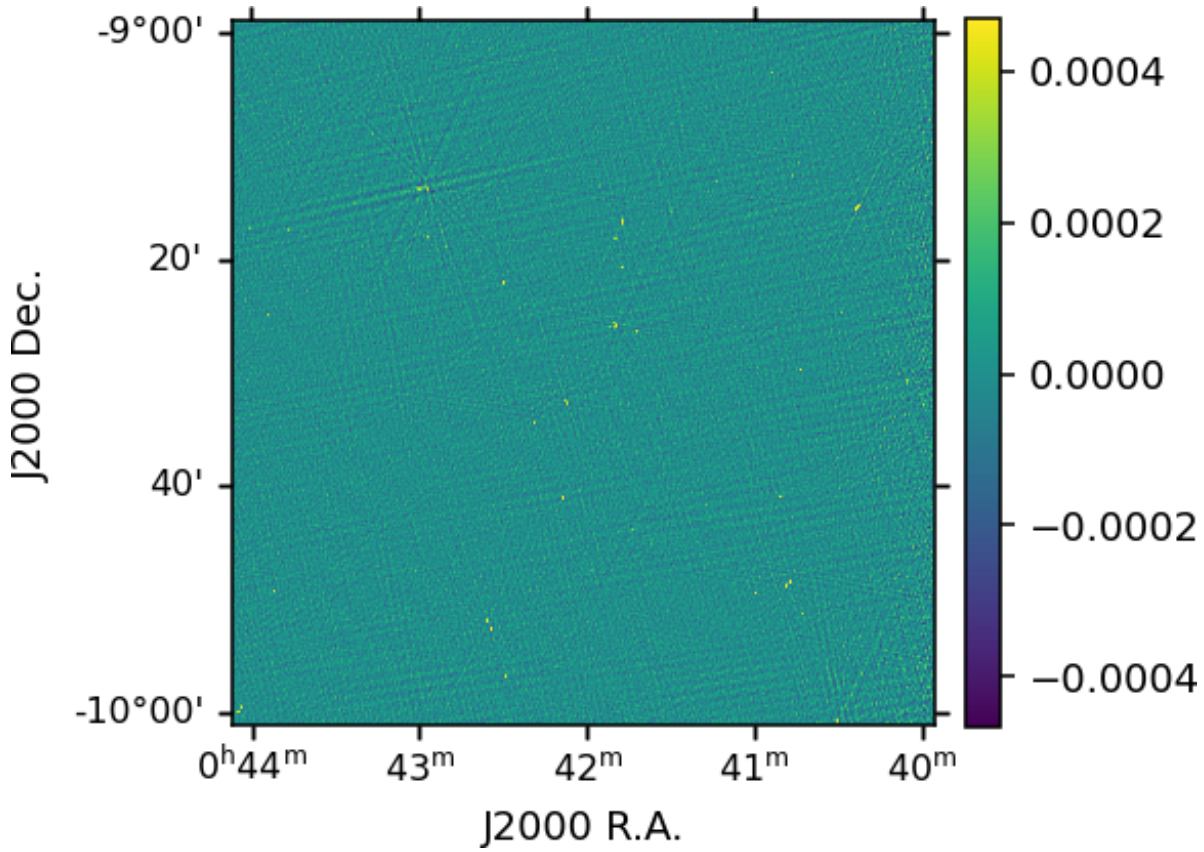

Figure 11: VLASS2 SE map. The image is convolved with a common beam of $3.23'' \times 2.27''$, PA $= 15.89°$. The unit of the colorbar is Jy beam^{-1}.

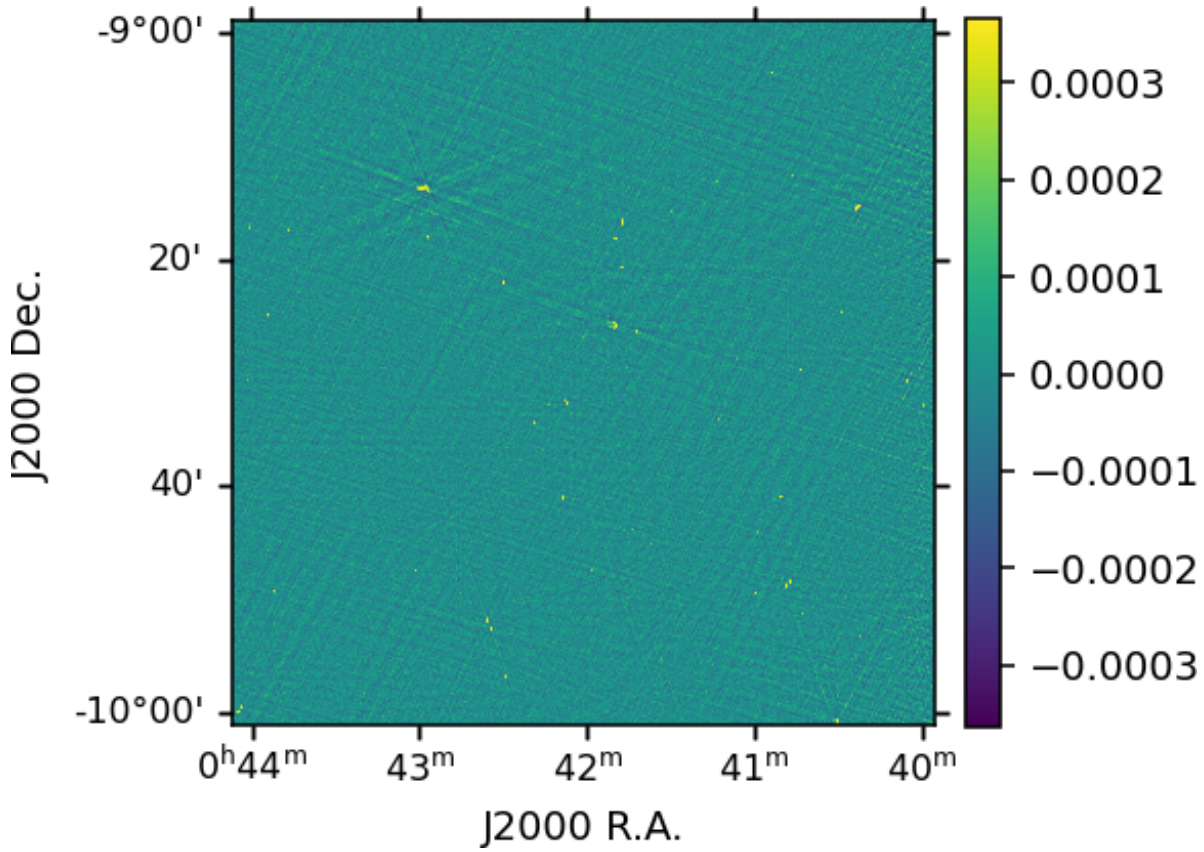

Figure 12: VLASS3 SE map. The image is convolved with a common beam of $3.23'' \times 2.27''$, PA $= 15.89°$. The unit of the colorbar is Jy beam^{-1}.

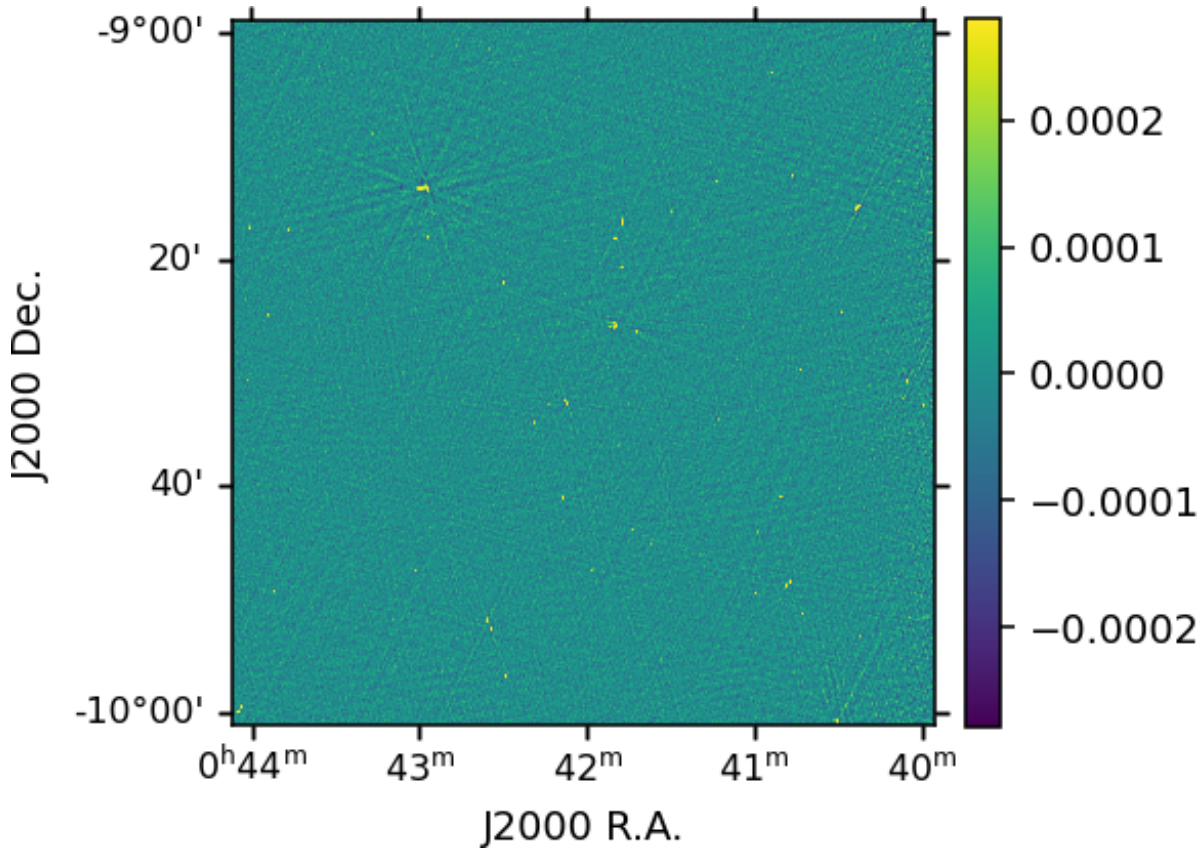

Figure 13: RMS-weighted mean SE map. The image is convolved with a common beam of $3.23'' \times 2.27''$, PA $= 15.89°$. The unit of the colorbar is Jy beam^{-1}.

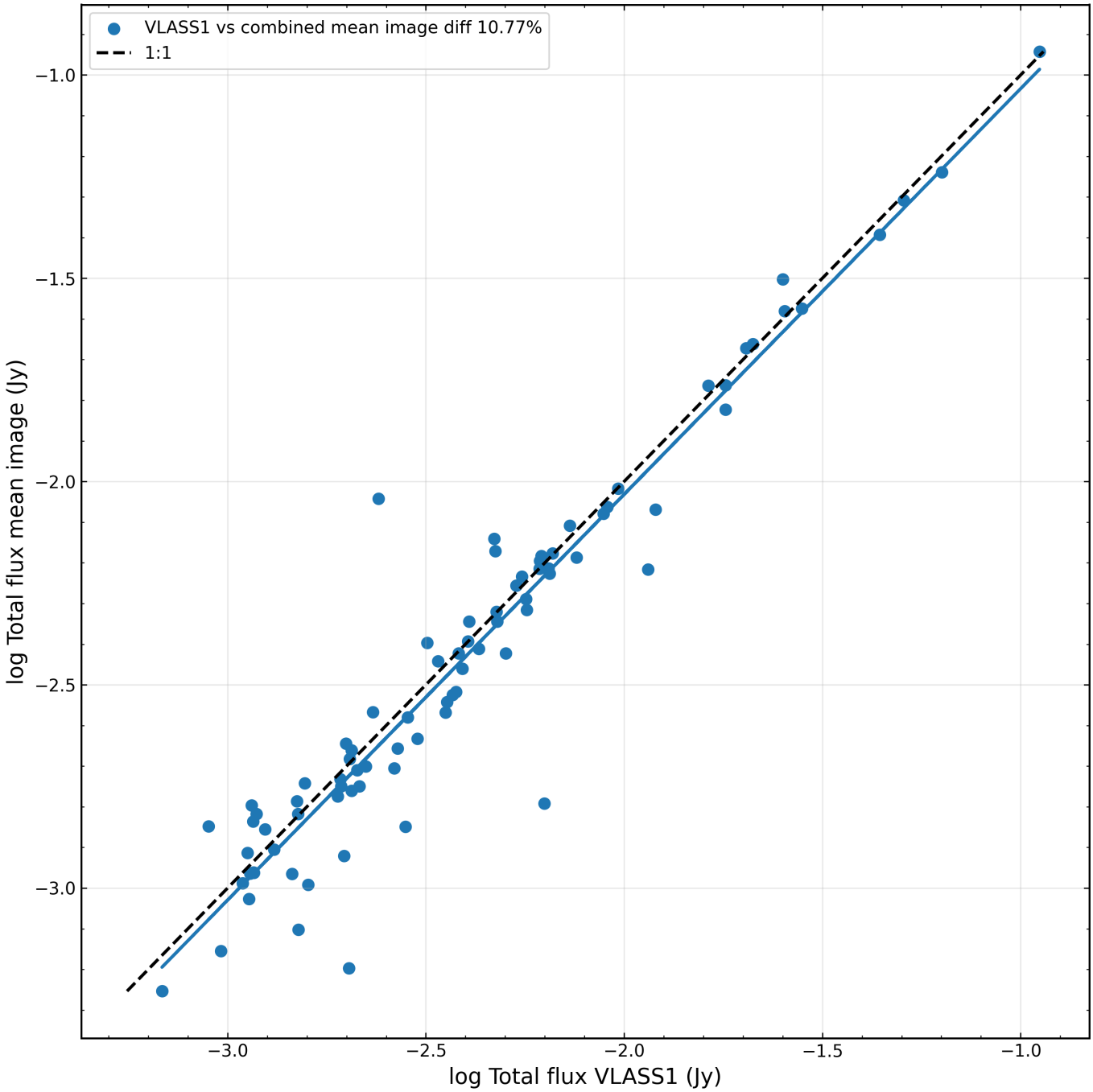

Figure 14: Flux densities comparisons between VLASS epoch 1 (QL) and combined mean maps.

Table 3: VLASS 1° QL maps RMS values. The beam size of each map is 3.78″ × 2.32″, 20.48°.

VLASS QL maps	RMS (mJy beam^{-1})	RMS ratio (to mean/to median)	Peak (mJy beam^{-1})	DR (Peak/RMS)
VLASS1	0.136	1.66/1.31	83	610
VLASS2	0.240	2.93/2.31	92	383
VLASS3	0.175	2.13/1.68	100	571
VLASS4	0.164	2.00/1.58	85	518
RMS-weighted mean	0.082		89	1085
RMS-weighted median	0.104		85	817

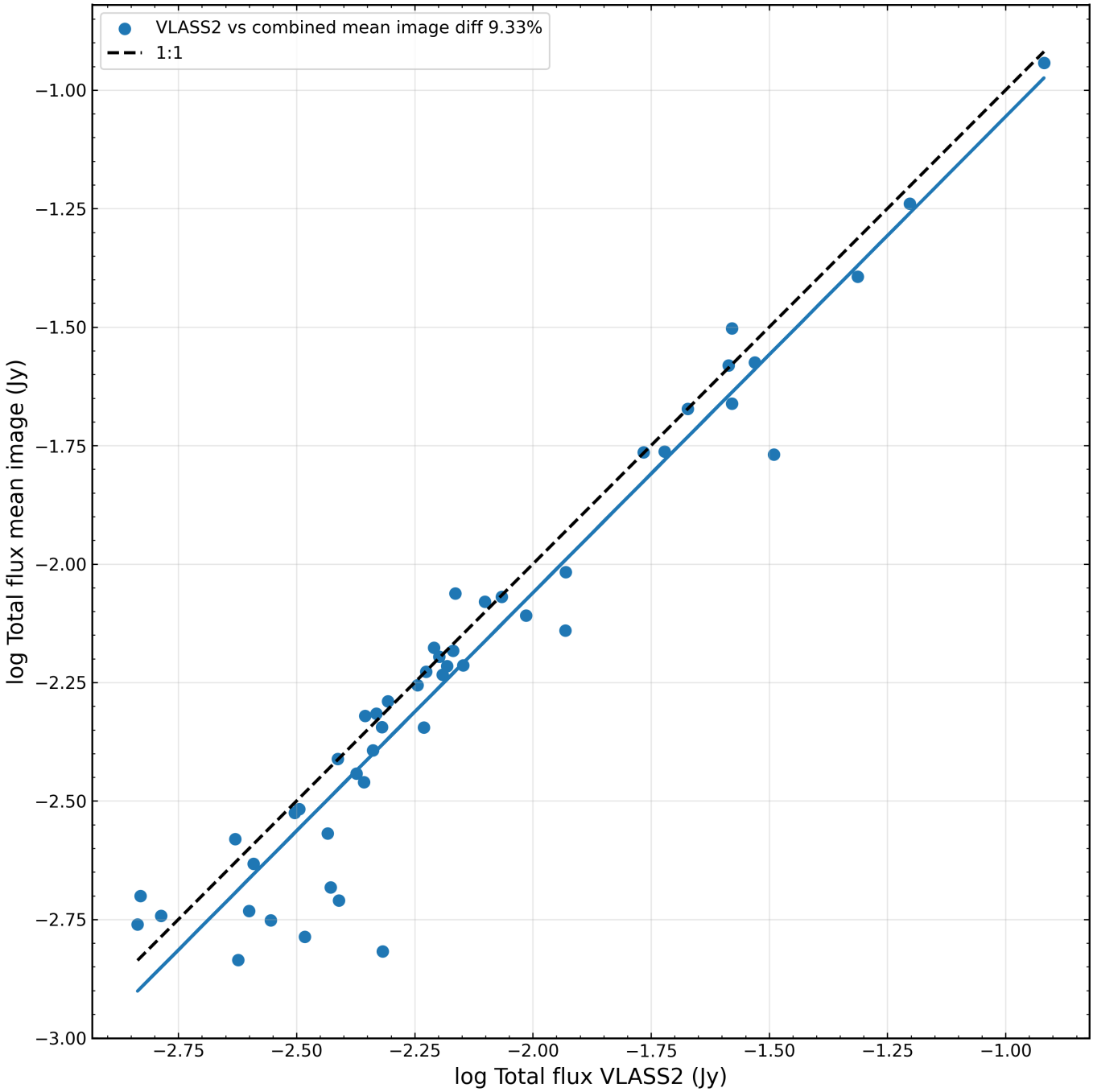

Figure 15: Flux densities comparisons between VLASS epoch 2 (QL) and combined mean maps.

6.2.2 VLASS SE maps

For the self-calibrated SE maps, we compared the available VLASS2 and VLASS3 single epoch maps with the weighted mean map using the total flux, island total flux, and peak flux values.

For the total flux, both SE epochs showed good agreement with the weighted mean map. The mean percentage difference was 5.68% for VLASS2 and 6.11% for VLASS3. The median ratios were 0.958 for VLASS2 and 1.019 for VLASS3, showing that the mean combined map is slightly fainter than VLASS2 but slightly brighter than VLASS3 in total flux. These values are close to unity in both cases, indicating that the SE mean map reproduces the integrated source flux scale well for both epochs.

For the island total flux, VLASS3 showed better agreement with the mean combined

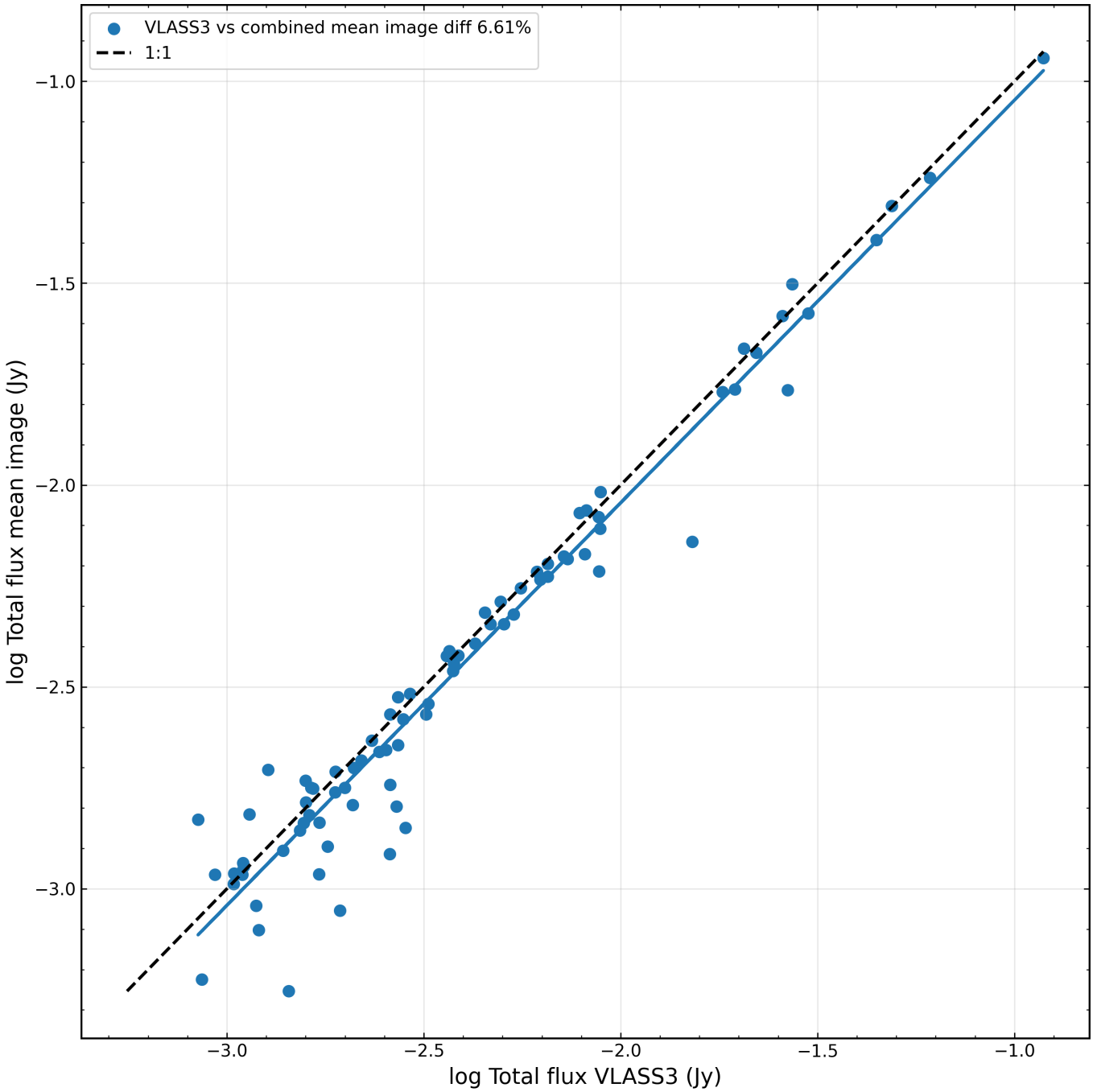

Figure 16: Flux densities comparisons between VLASS epoch 3 (QL) and combined mean maps.

map than VLASS2. The mean percentage difference was 12.04% for VLASS2 and 5.44% for VLASS3. The median ratios were 1.005 for VLASS2 and 1.056 for VLASS3. This suggests that the island-scale emission in the combined SE map is very close to VLASS2 and modestly higher than VLASS3. The larger island-flux difference for VLASS2 may reflect differences in how extended or blended emission is defined between that epoch and the stacked map.

For peak flux, the agreement was especially strong. The mean percentage difference was only 0.72% for VLASS2 and 0.11% for VLASS3. The median ratios were 0.973 for VLASS2 and 1.000 for VLASS3, showing that the combined SE map closely matches the peak-brightness scale of both epochs, with an almost exact match for VLASS3. Among all SE comparisons, peak flux gives the tightest agreement with the mean combined map.

Taken together, these results show that the weighted mean SE combined map matches

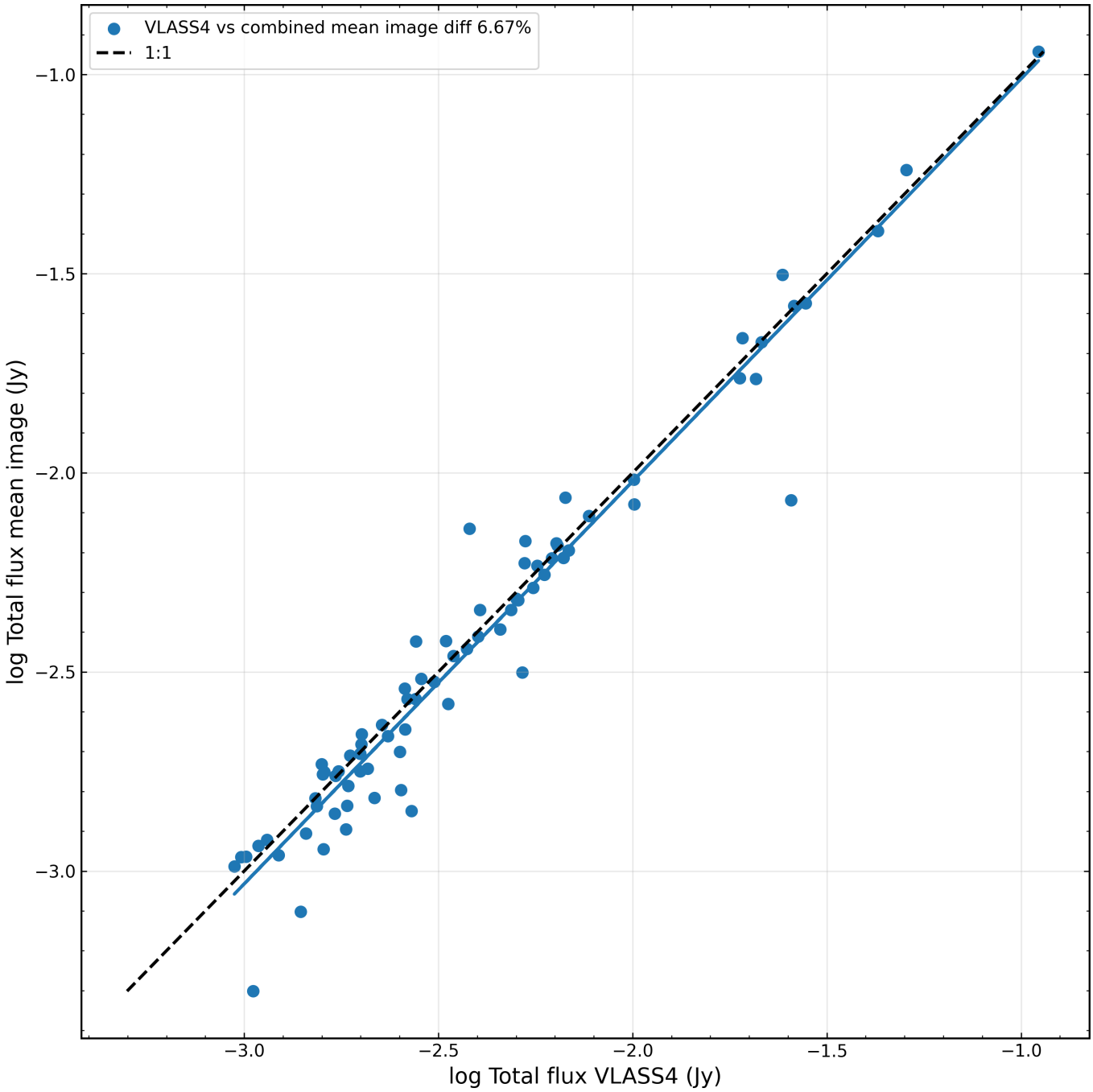

Figure 17: Flux densities comparisons between VLASS epoch 4 (QL) and combined mean maps.

both available SE epochs very well, especially for peak flux. VLASS3 is slightly better matched in island total flux and peak flux, while VLASS2 is slightly better matched in total flux. In general, the SE mean map appears to preserve both integrated and peak source properties well, with the strongest consistency seen in peak flux. We plotted total, peak, and island fluxes for VLASS SE individual epoch vs combined mean maps from Figs. 38 to 43. We listed all statistical values for SE maps in the Appendix Table 6.

6.2.3 VLASS SE alpha maps

The VLASS self-calibrated pipeline also provides an alpha map as a user data product in the archive, defined as the ratio of the Taylor coefficient 1 and Taylor coefficient 0 maps (tt1/tt0). For the SE data shown above, we downloaded the corresponding tt1 maps for VLASS epochs

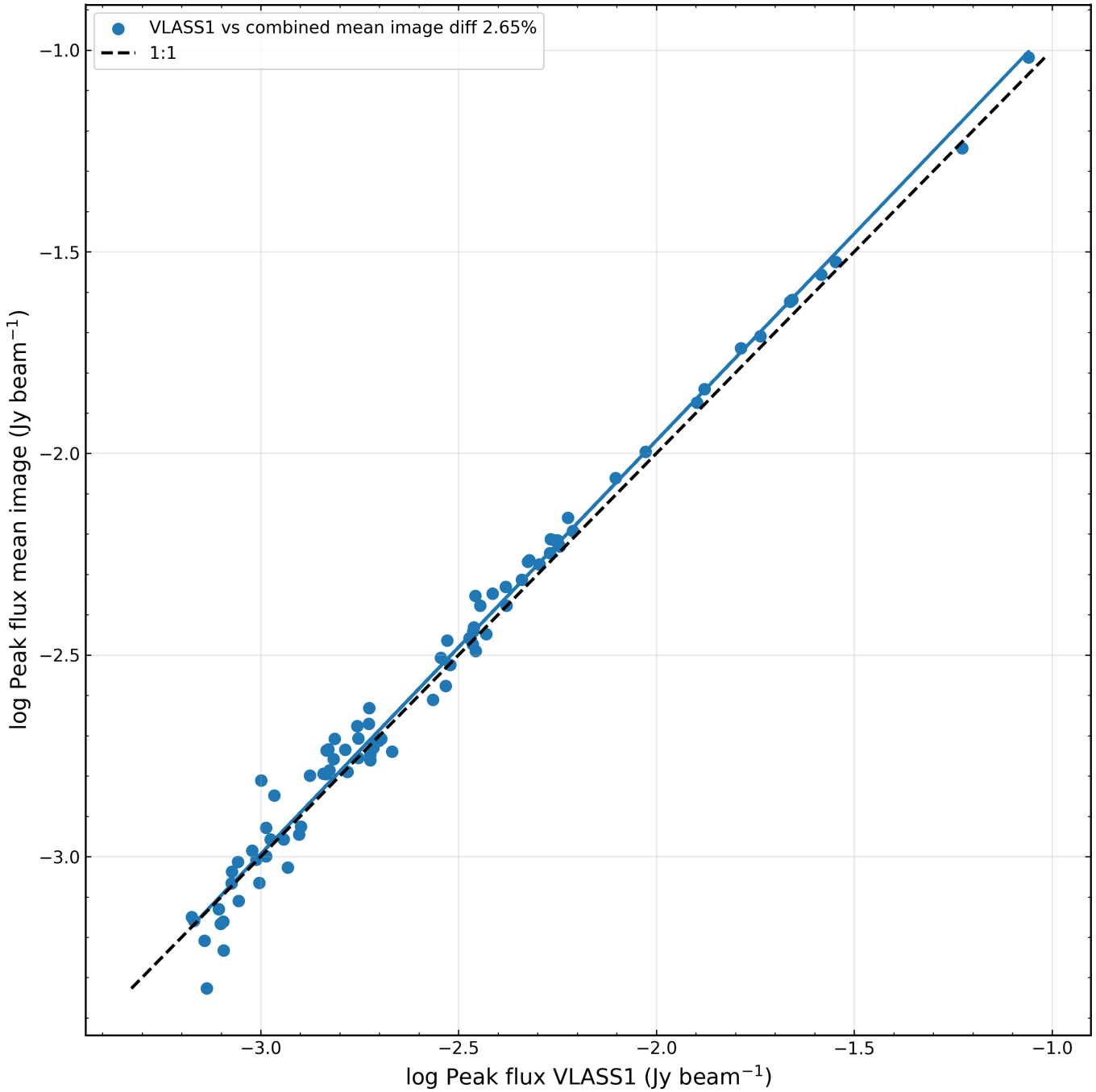

Figure 18: Peak flux comparisons between VLASS epoch 1 (QL) and combined mean maps.

Table 4: VLASS 1° SE maps RMS values. The beam size of each map is 3.23″ × 2.27″, 15.89°.

VLASS SE maps	RMS (mJy beam^{-1})	RMS ratio (to mean)	Peak (mJy beam^{-1})	DR (Peak/RMS)
VLASS2	0.191	1.68	96	502
VLASS3	0.150	1.32	98	653
RMS-weighted mean	0.114		97	850

2 and 3. We then combined these tt1 maps in the same manner as the tt0 maps, using regridding, convolution to a common beam, and RMS-weighted mean combination. From these products, we generated a combined alpha map as `combined_tt1/combined_tt0`. We then masked low-SNR pixels in the combined alpha map to display the radio sources more clearly. In Fig. 44, we show cutouts of the combined alpha map for a few radio sources and

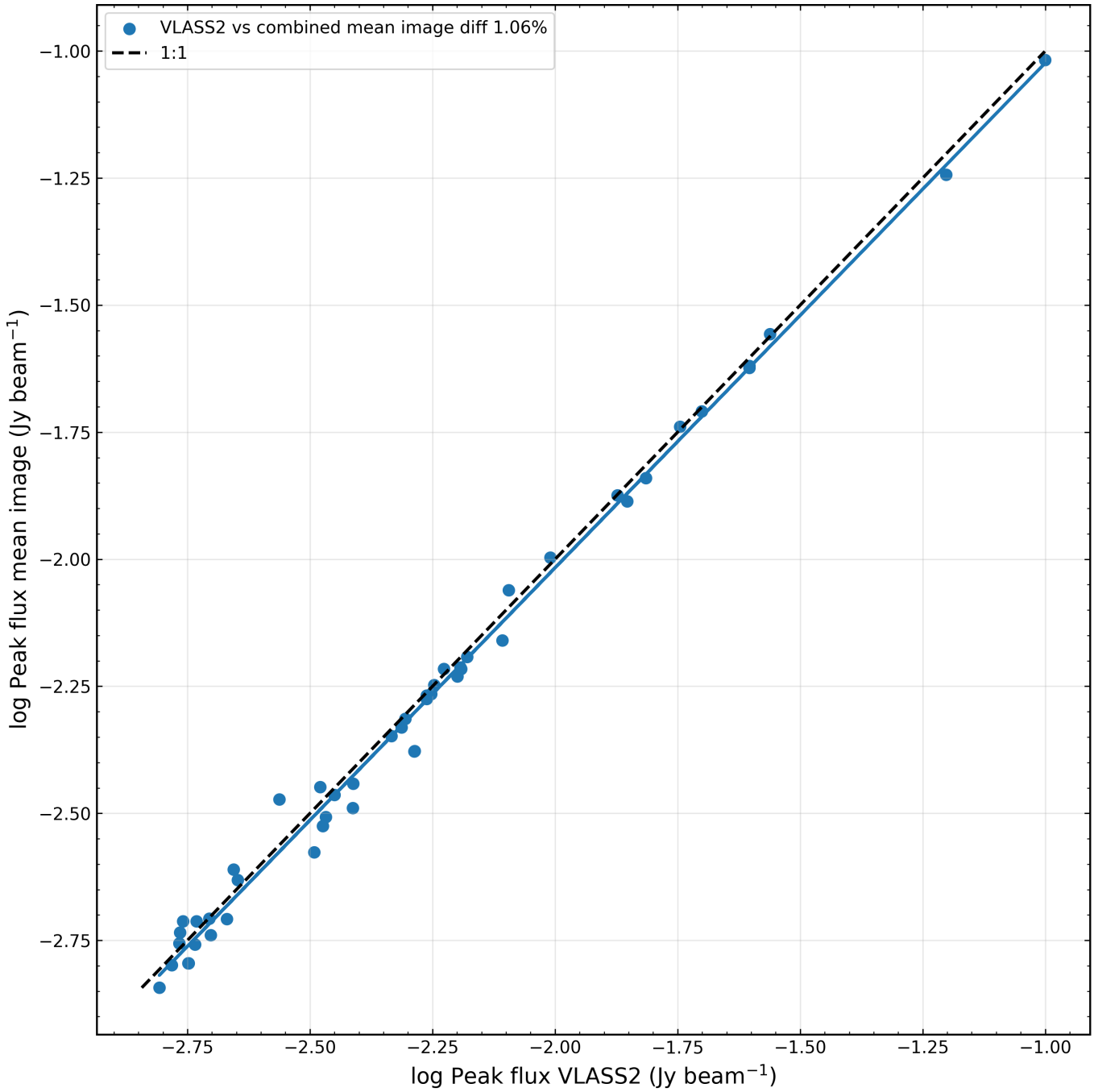

Figure 19: Peak flux comparisons between VLASS epoch 2 (QL) and combined mean maps.

compare them with the corresponding single-epoch alpha maps.

7 Discussion and Conclusions

In our cutout image combination analysis (§ 6.1), the RMS noise measurements show that the common-beam image stacking improves the noise performance relative to the individual VLASS epoch images. For the QL (cutout) maps (Table 1), the single-epoch RMS values are 0.140, 0.188, 0.165, and 0.141 mJy beam^{-1}, giving an average single-epoch RMS of 0.158 mJy beam^{-1}. The RMS-weighted mean combined map has an RMS of 0.089 mJy beam^{-1}, corresponding to an overall improvement by a factor of ∼1.78 relative to the average single-epoch QL image. The RMS-weighted median map has an RMS of 0.112 mJy beam^{-1}, corresponding to an improvement by a factor of ∼1.42. Even relative to the best individual

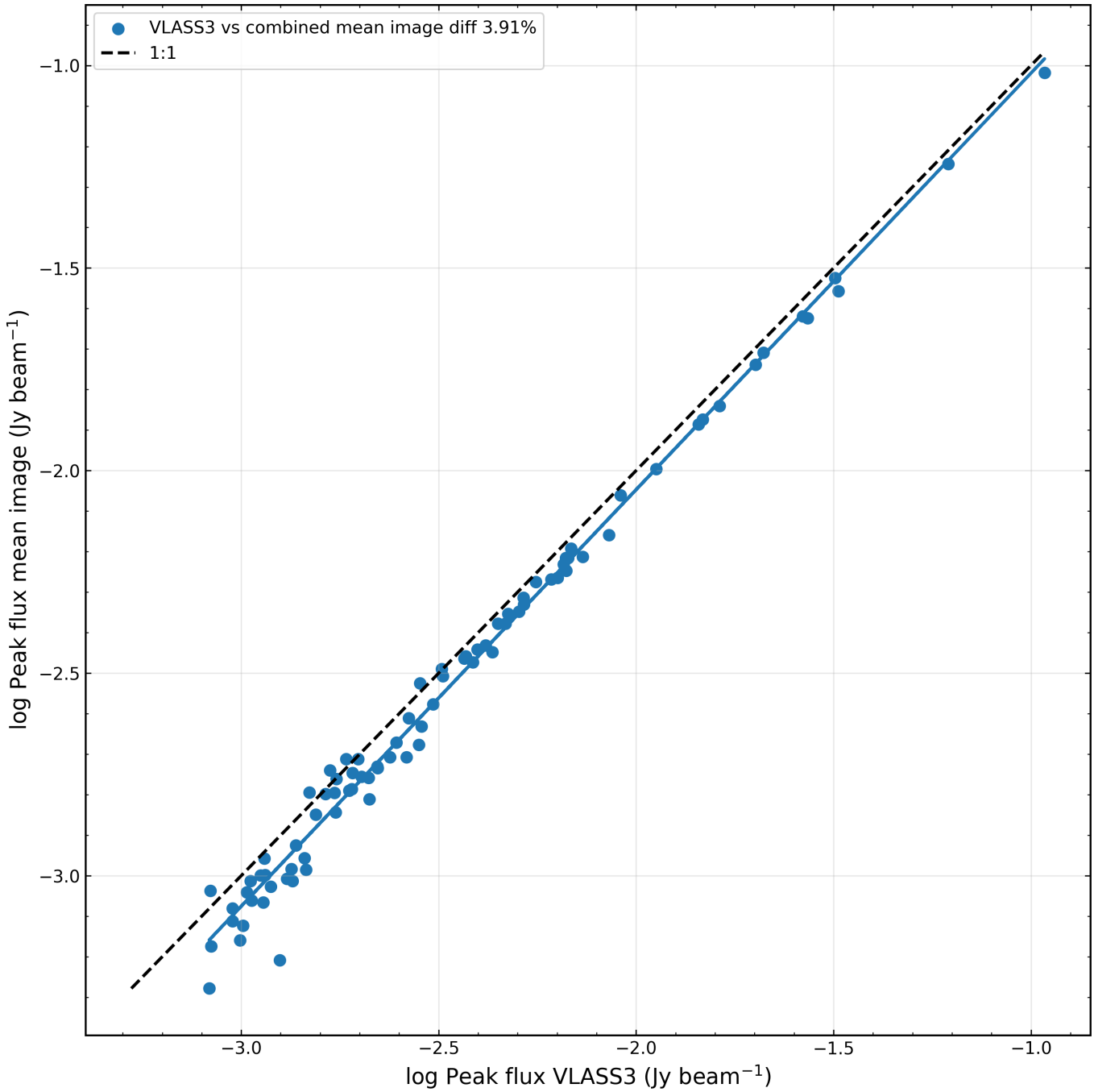

Figure 20: Peak flux densities comparisons between VLASS epoch 3 (QL) and combined mean maps.

QL epoch (0.140 mJy beam^{-1}), the weighted-mean map still improves the RMS by a factor of ∼1.57, while the weighted-median map improves it by a factor of ∼1.25. A similar trend is seen for the corresponding SE (cutout) maps (Table 2). Using the single-epoch SE RMS values of 0.166 and 0.155 mJy beam^{-1}, the average single-epoch RMS is 0.160 mJy beam^{-1}. The RMS-weighted mean SE combined map has an RMS of 0.115 mJy beam^{-1}, corresponding to an improvement by a factor of ∼1.40 relative to the average single-epoch SE image. Relative to the best individual SE image (0.155 mJy beam^{-1}), the weighted-mean map improves the RMS by a factor of ∼1.35. We also calculate dynamic range for both QL and SE maps, and it shows there is a factor of ∼ 2 improvements in combined maps.

As shown in § 6.2.1 and § 6.2.2, for full VLASS QL maps (Table 3), the average RMS for four epochs is ∼ 0.178 mJy beam^{-1}. The combined mean and median maps are improving

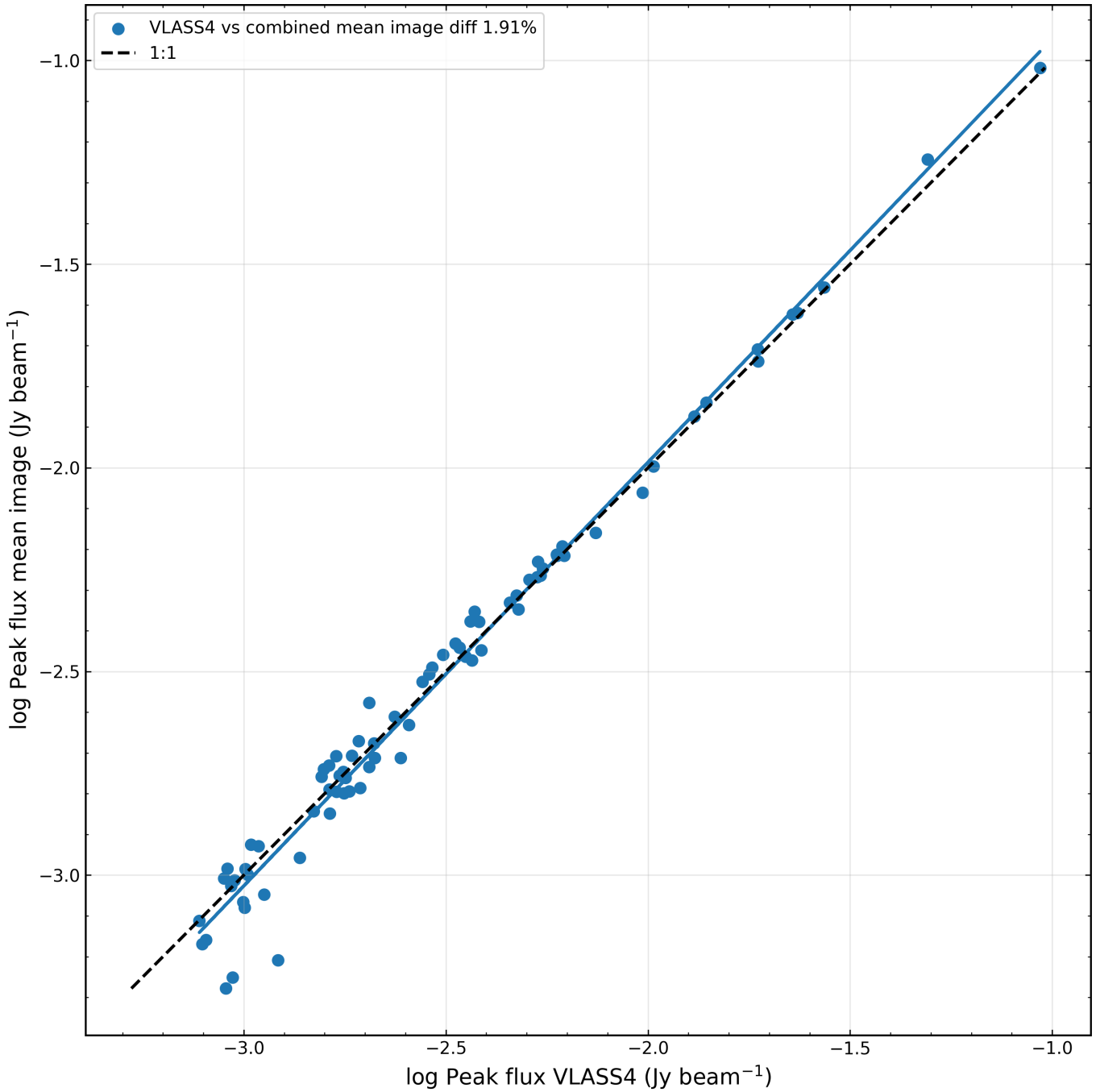

Figure 21: Peak flux comparisons between VLASS epoch 4 (QL) and combined mean maps.

RMS by a factor of 2 and 1.7, respectively. For VLASS SE images (Table 4), we found RMS improvements of ∼1.50 for the mean image compared to the average RMS of epoch 2 and 3 maps. In both of these maps, dynamic range is also improved by a factor of ∼ 1.5 to 2 for combined maps.

These results show that the RMS-weighted mean combination gives the strongest improvement in sensitivity for both QL and SE data. This is expected because the weighted mean makes fuller use of the lower-noise measurements and therefore suppresses the contribution from noisier epochs more efficiently. The weighted median, while still useful, provides a smaller gain in RMS because it is designed to be more robust to outliers and localized bad measurements rather than to maximize sensitivity. In other words, the weighted mean is better for achieving the lowest background noise, whereas the weighted median is better for resisting the influence of occasional problematic pixels or residual image artifacts. The

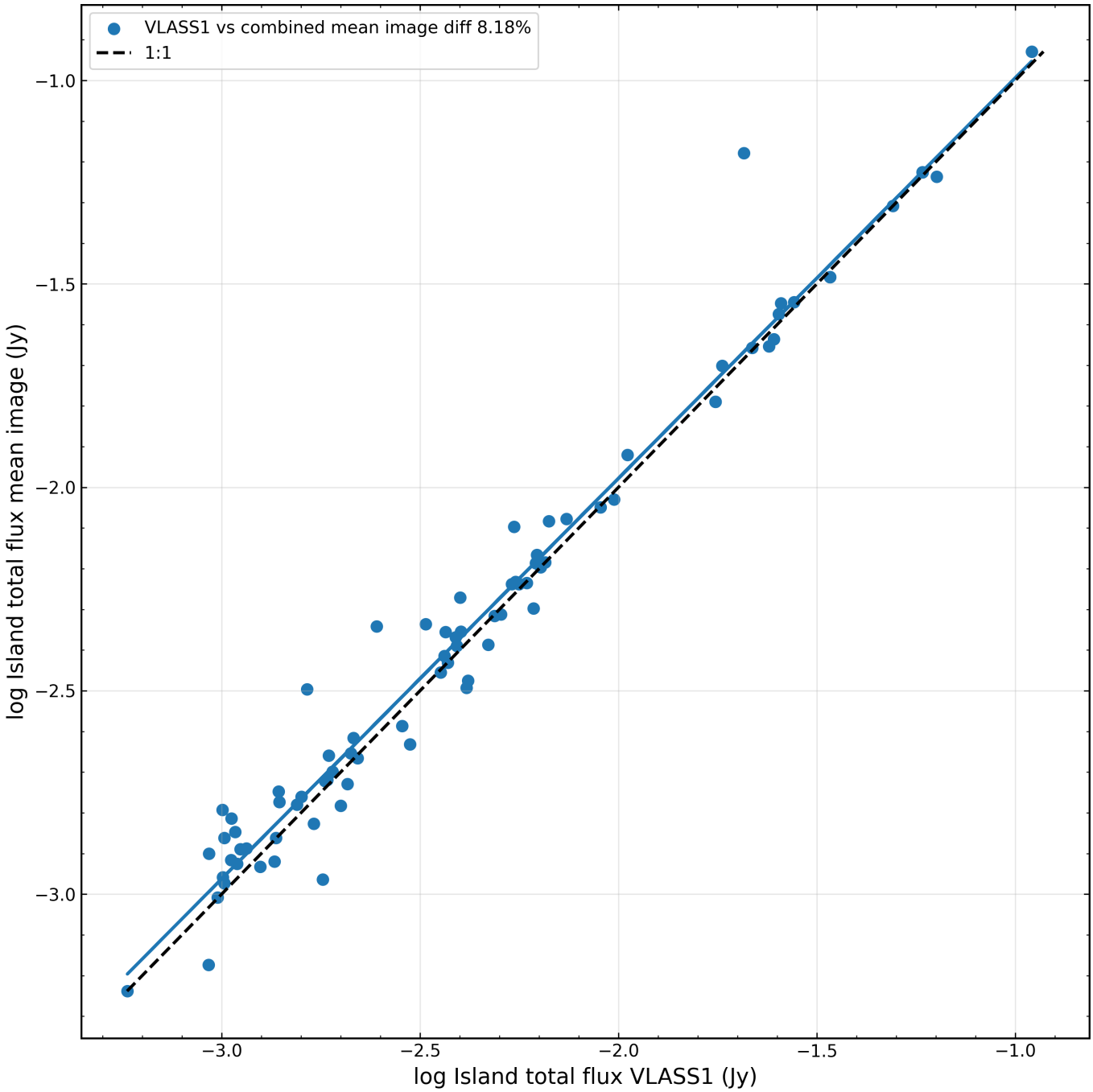

Figure 22: Island flux comparison between VLASS epoch 1 (QL) and combined mean maps.

larger improvement seen for the QL maps compared to the SE maps may reflect the fact that the QL epoch images show a wider range of RMS values, so the local RMS weighting can more effectively downweight the noisier inputs. For the SE maps, where the two epochs are already closer in RMS, the overall gain from combination is naturally smaller. Even so, the combined maps still provide a more stable image product than the individual epochs alone.

We also compared fluxes for QL and SE maps with their respective combined products. Mainly, we noticed that the combined maps are generally closer to the later VLASS epochs 3 and 4 than to the earlier ones (1 and 2). The overall differences between individual and combined fluxes (total, peak, and island) arise from a combination of effects, including changes in beam shape, resolution, local noise, and source segmentation between epochs. Such effects can redistribute emission between the source peak and more extended structure, which would affect peak flux more strongly than total flux. Differences in PyBDSF island

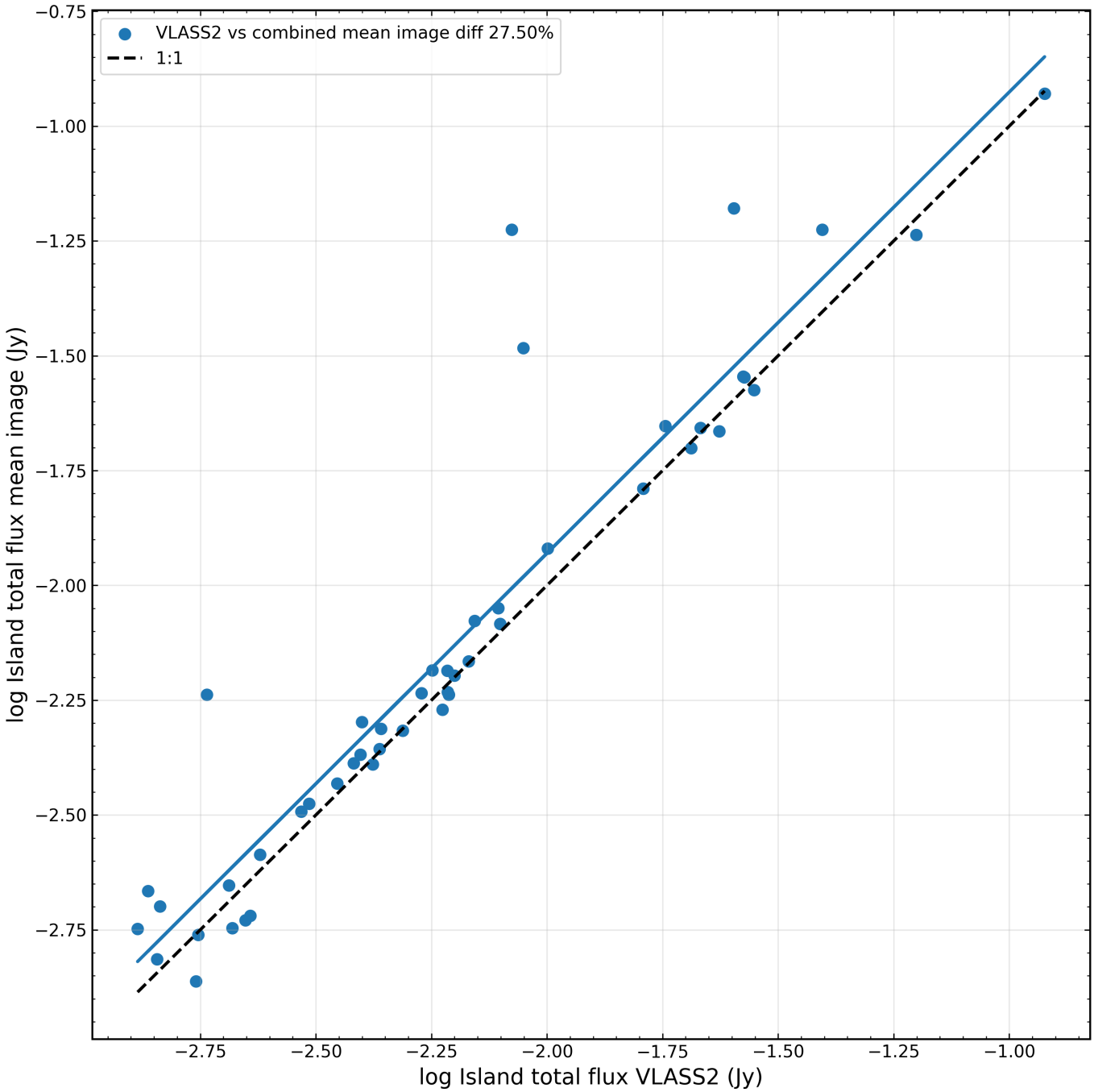

Figure 23: Island flux comparison between VLASS epoch 2 (QL) and combined mean maps.

definitions may also contribute, especially for blended or extended sources. The important result is the fact that the island total fluxes ratios were usually > 1, for both QL (mean and median) and SE maps, indicating that the combined maps tend to recover a little more island-scale emission than the single-epoch maps. This is due to the better sensitivities of combined mean and median maps as suggested above RMS analysis. It should be noted that these results may vary depending on the specific VLASS QL and SE maps analyzed.

Comparing the QL and SE results, the SE maps show better agreement with the combined map than the QL maps in most cases. This is most obvious for peak flux, where the SE mean percentage differences are extremely small (0.72% for VLASS2 and 0.11% for VLASS3), and the median ratios are very close to 1. The total-flux agreement is also strong for the SE maps, with mean percentage differences near 6%, which is comparable to or better than the best QL cases. These results are consistent with the fact that the SE images are self-

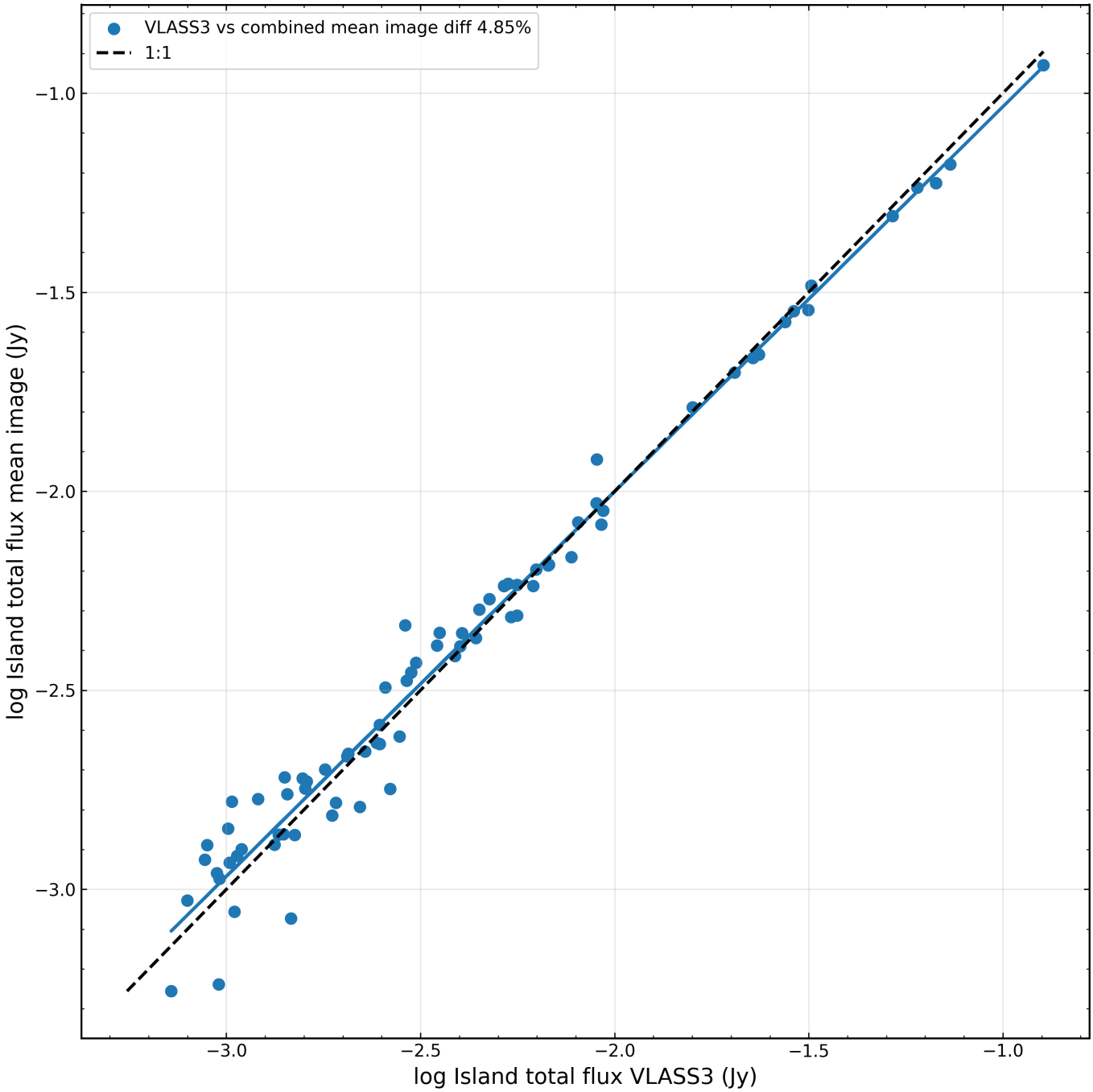

Figure 24: Island flux comparison between VLASS epoch 3 (QL) and combined mean maps.

calibrated and therefore have more stable flux recovery, cleaner source structure, and better image fidelity. As a result, the SE combined map more closely tracks the individual epochs, while the QL combined maps show somewhat larger offsets, especially in island total flux and in peak flux for some epochs.

We also note that in these our tests (for both QL and SE), adding a 10% padding to the common beam (generated by radio-beam) produced a sufficiently larger target beam, so the direct convolution in Jy beam^{-1} and the Jy beam^{-1} $\rightarrow$ K $\rightarrow$ Jy beam^{-1} approach gave consistent flux densities. This indicates that, when the target beam is safely larger than the input beams, an explicit unit conversion is not strictly required for flux preservation. However, in this experiment we chose to convolve using the radio-beam-derived common beam, which is closer to the limiting deconvolvable beam. Therefore, we converted the images from Jy beam^{-1} to K before convolution and then back to Jy beam^{-1} using the

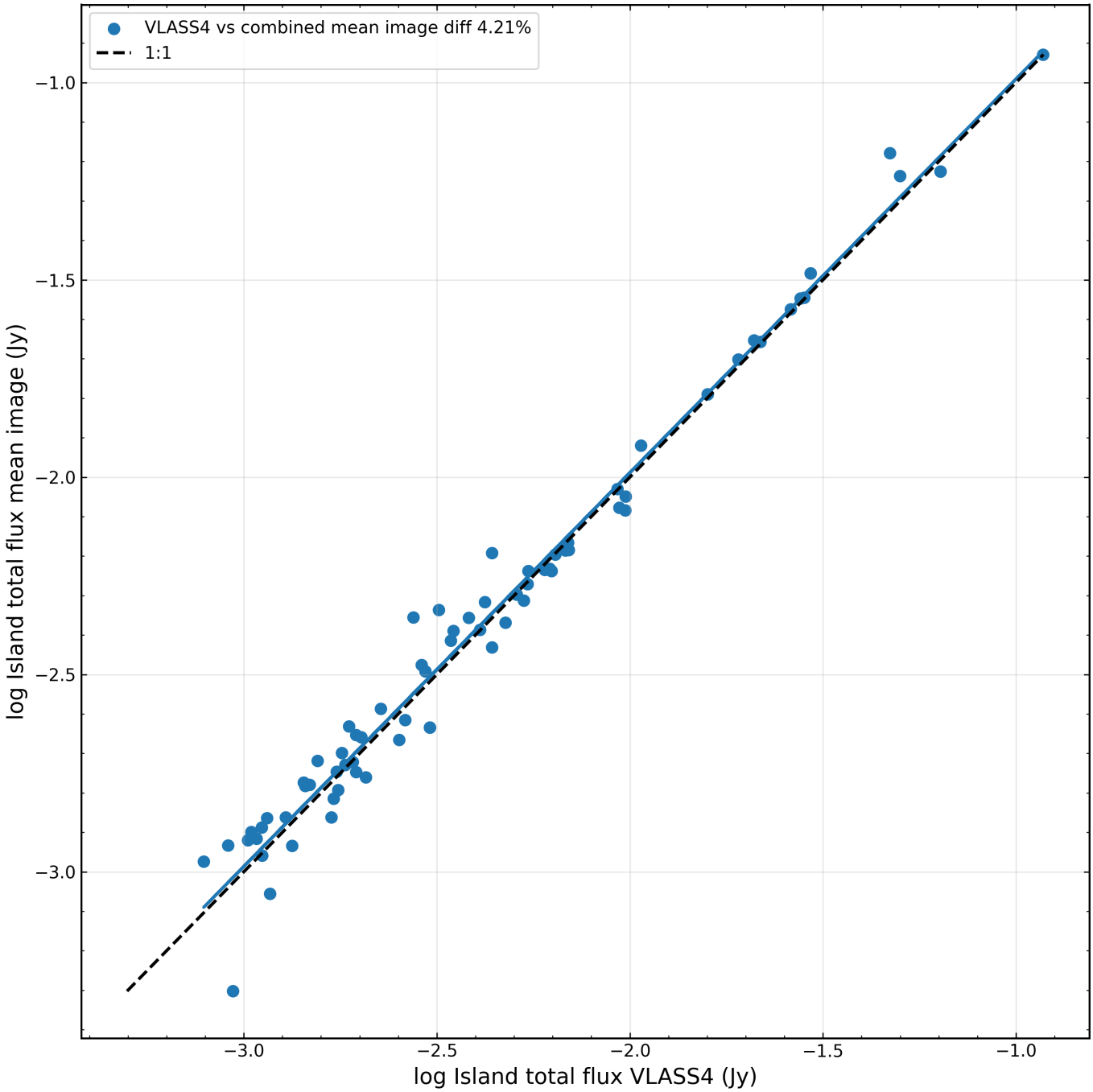

Figure 25: Island flux comparisons between VLASS epoch 4 (QL) and combined mean maps.

target beam, so that the smoothing is applied to a surface-brightness-like quantity and the final images have the correct beam-dependent flux-density scaling.

Overall, the beam-matched RMS-weighted combination appears to work as intended. The common-beam smoothing ensures that all epoch images are compared and combined at the same angular resolution, while the local RMS weighting improves the effective sensitivity by reducing the contribution from noisier regions and noisier epochs. The resulting weighted-mean maps provide the strongest improvement in noise performance, and the weighted-median maps provide a complementary product that is more sensitive to outliers. This makes the combined images useful for improving the detectability of faint emission and for producing more stable multi-epoch VLASS image products. We also shown combined alpha map for SE data using tt1 and tt0 convolved map. With improved sensitivity, the combined alpha map well represents the spectral indices of radio sources.

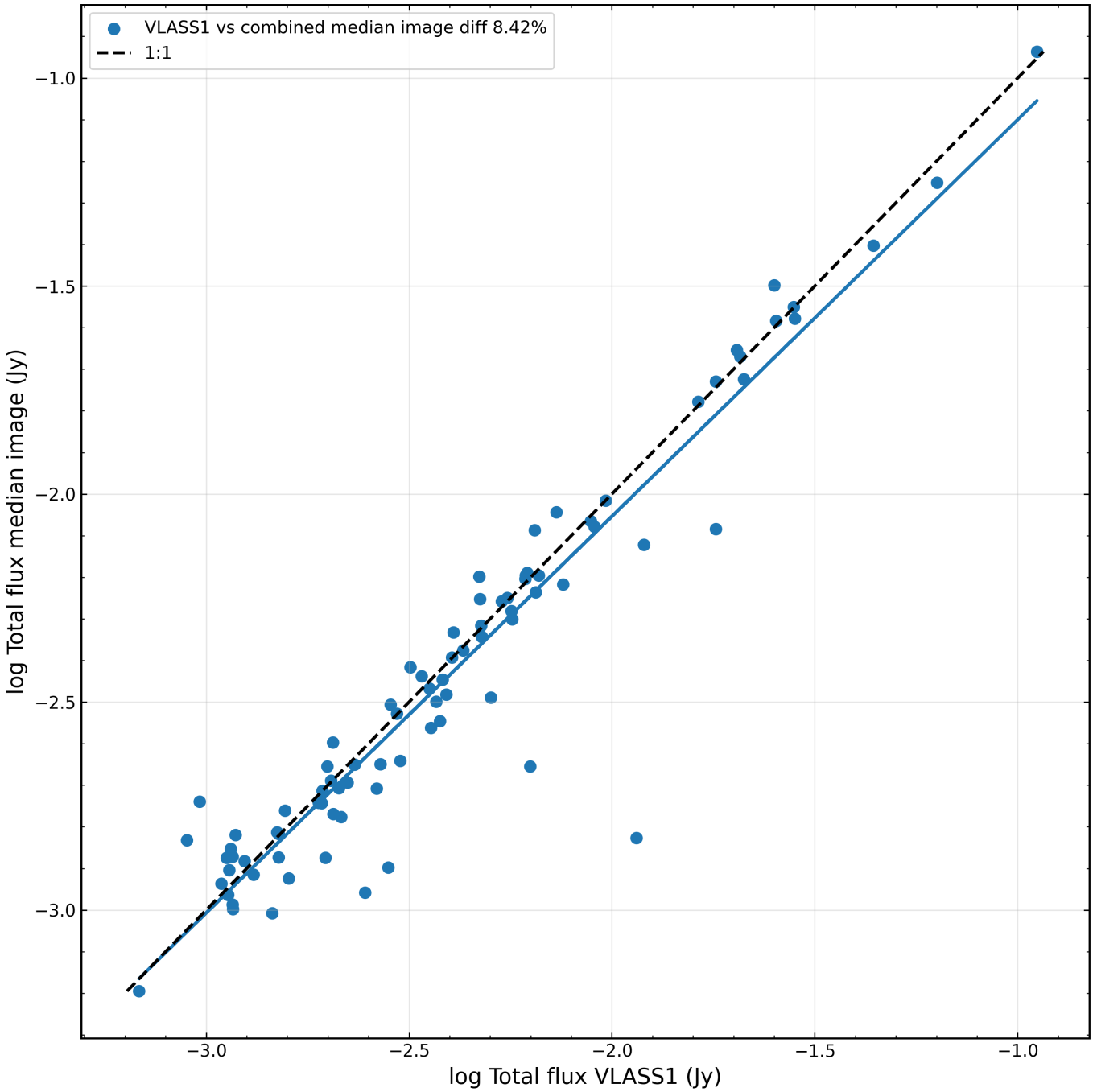

Figure 26: Flux densities comparisons between VLASS epoch 1 (QL) and combined median maps.

At present, our cutout server serves as a practical testing platform for VLASS image combination and visualization. In future work, additional features can be implemented, such as support for more automated source finding and flux measurement on the stacked products, user-selectable beam-matching and weighting options, improved artifact rejection, and direct comparison between QL and SE combined maps. The framework can also be extended to include multi-wavelength data cross matching and display images from other surveys, as well as VLASS spectral index (alpha) and polarization maps and cubes, integration of deconvolution-based or super-resolution image combination methods and possible to add more advanced visualization tools. This analysis provides a useful foundation for exploring multi-epoch VLASS image stacking and for developing improved tools for faint radio-source detection and characterization.

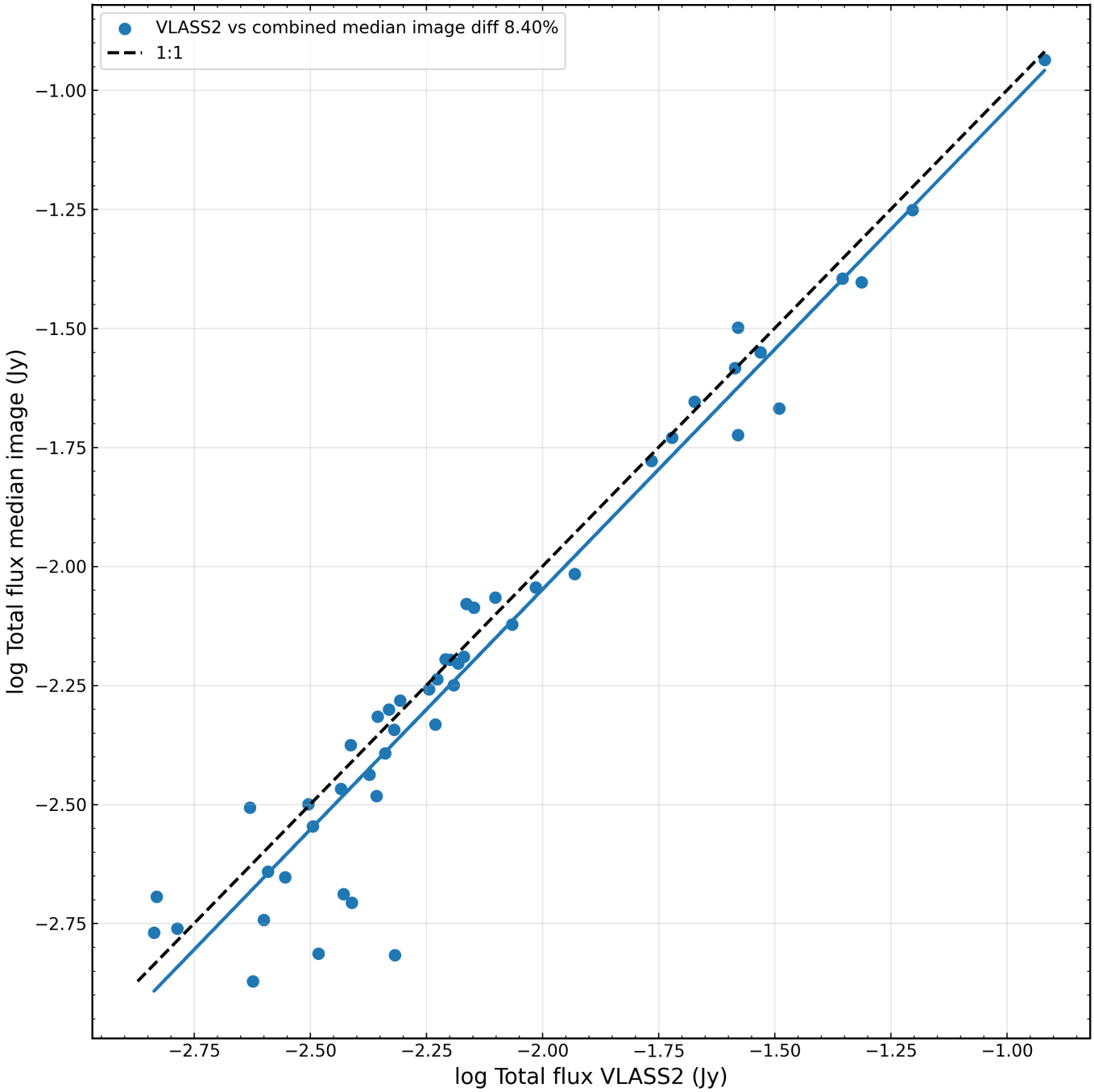

Figure 27: Flux densities comparisons between VLASS epoch 2 (QL) and combined median maps.

References

Lacy, M. et al. 2020, PASP, 132, 035001, 1907.01981

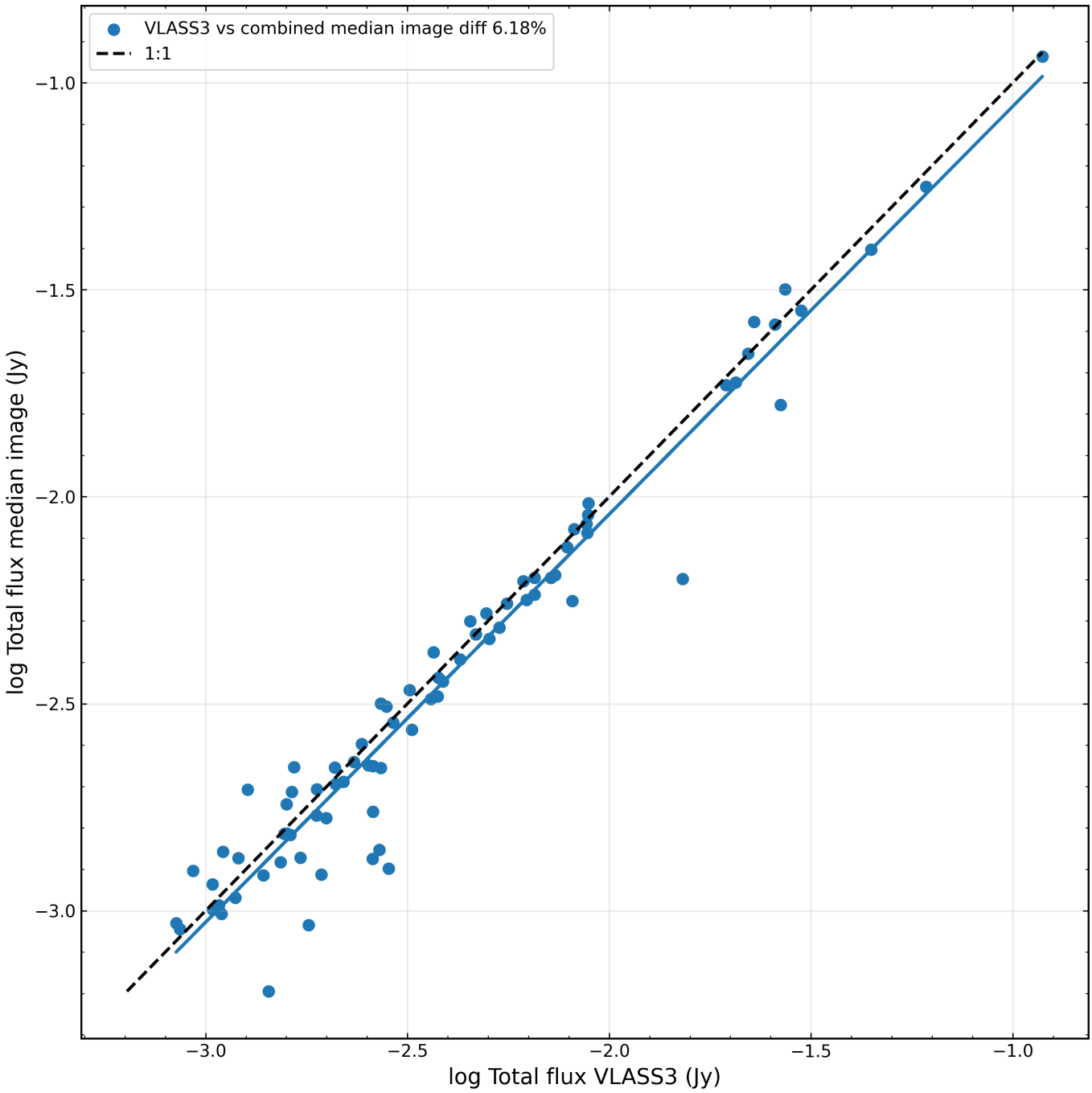

Figure 28: Flux densities comparisons between VLASS epoch 3 (QL) and combined median maps.

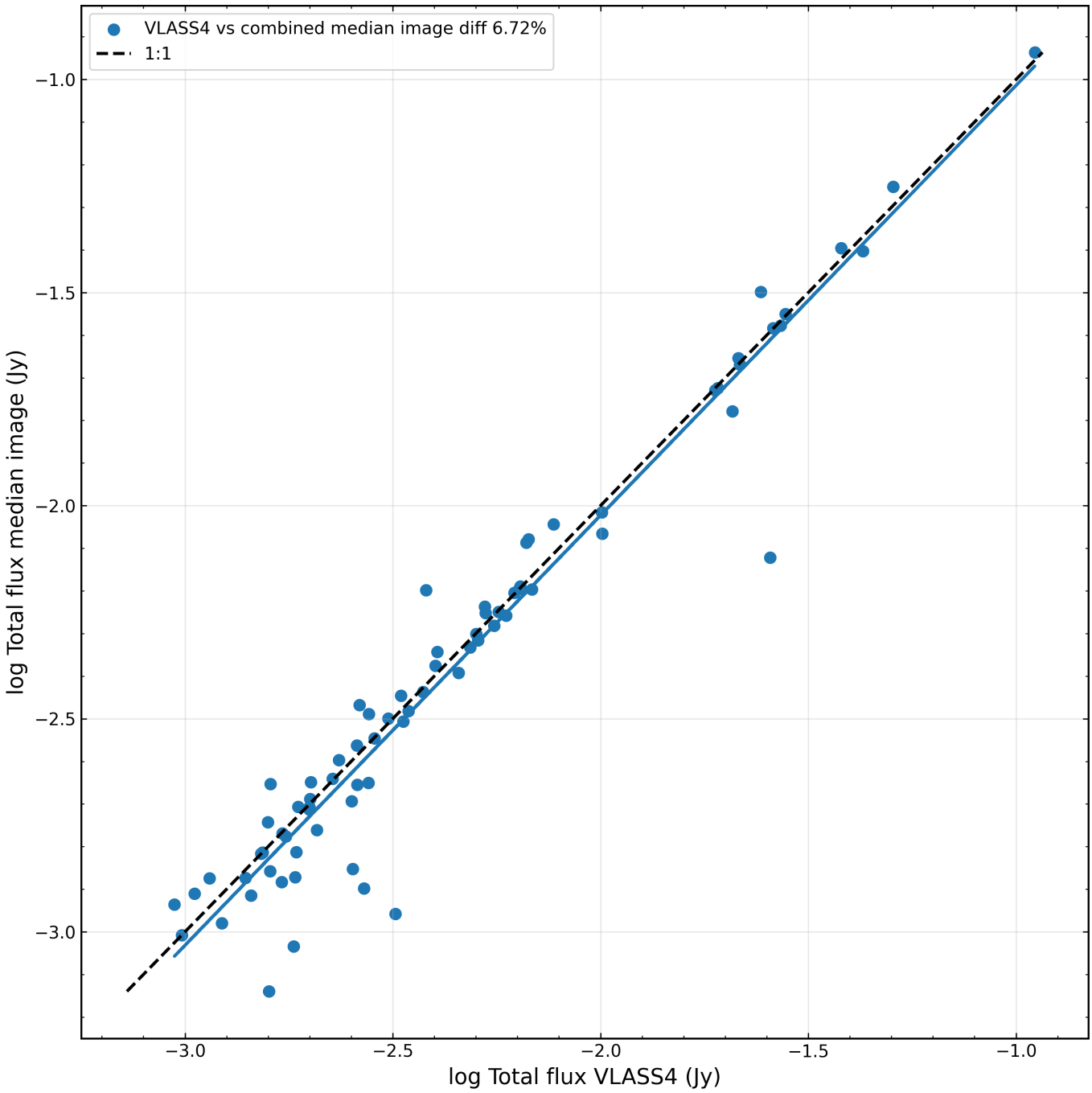

Figure 29: Flux densities comparisons between VLASS epoch 4 (QL) and combined median maps.

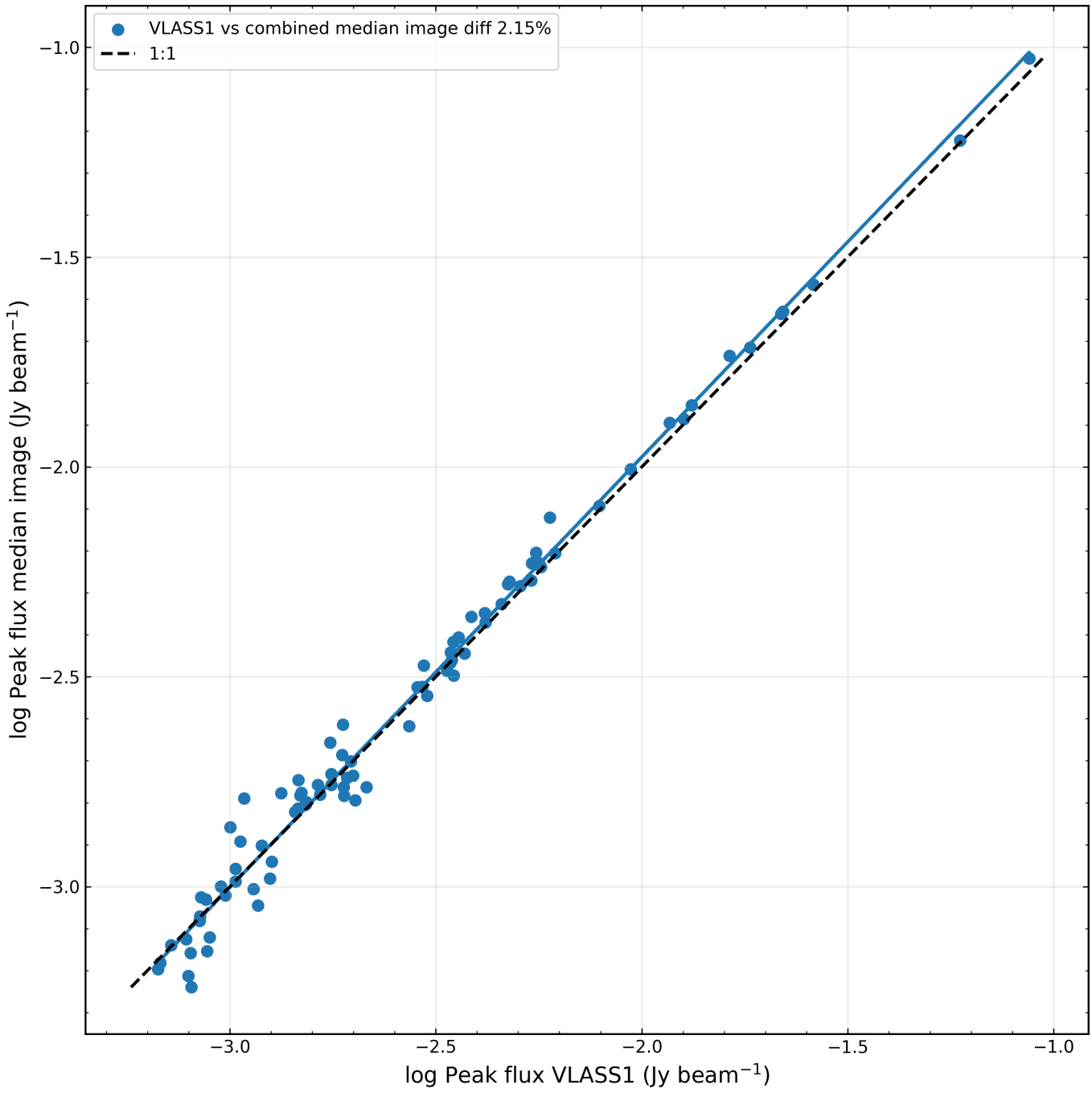

Figure 30: Peak flux comparisons between VLASS epoch 1 (QL) and combined median maps.

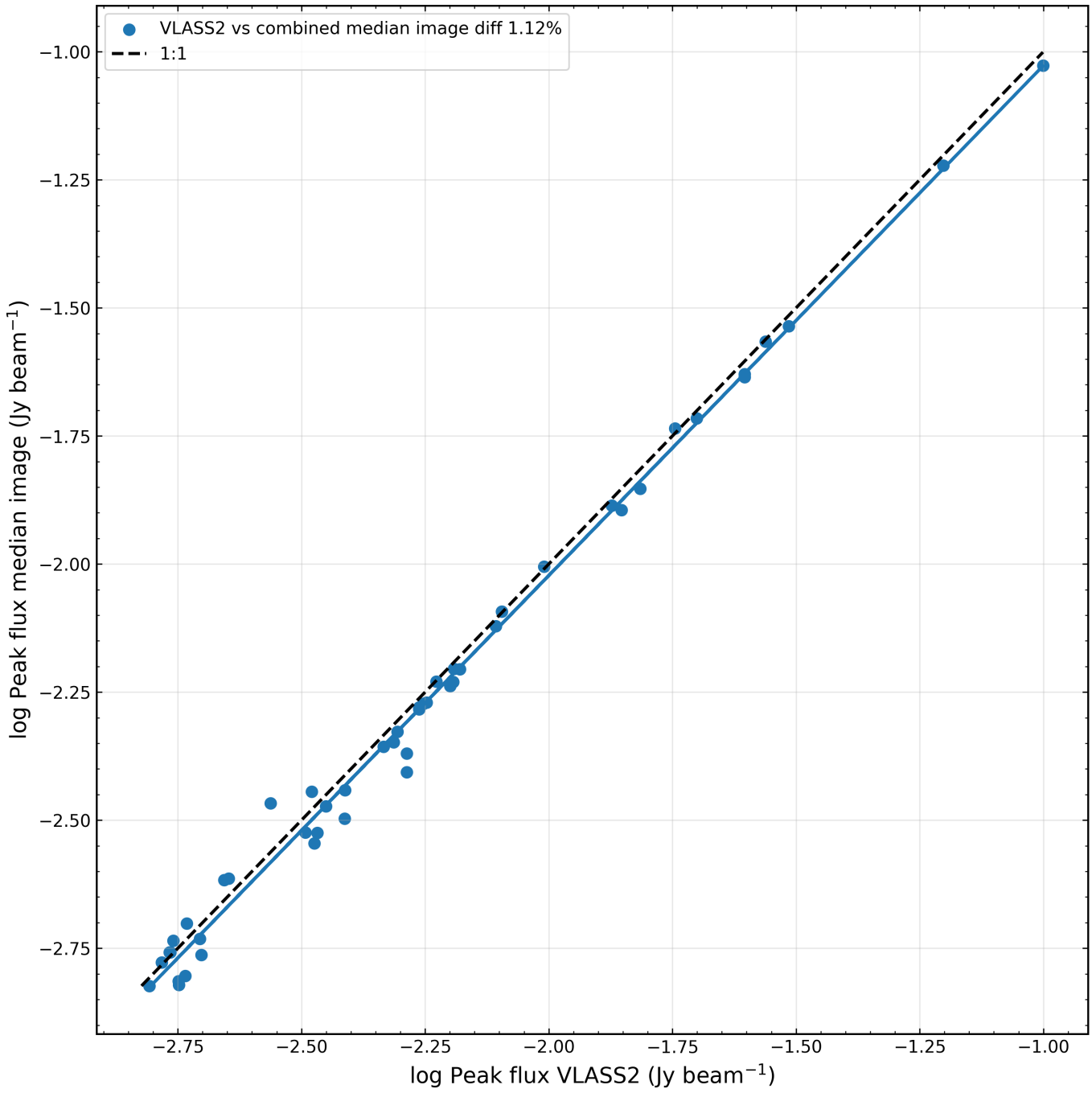

Figure 31: Peak flux comparisons between VLASS epoch 2 (QL) and combined median maps.

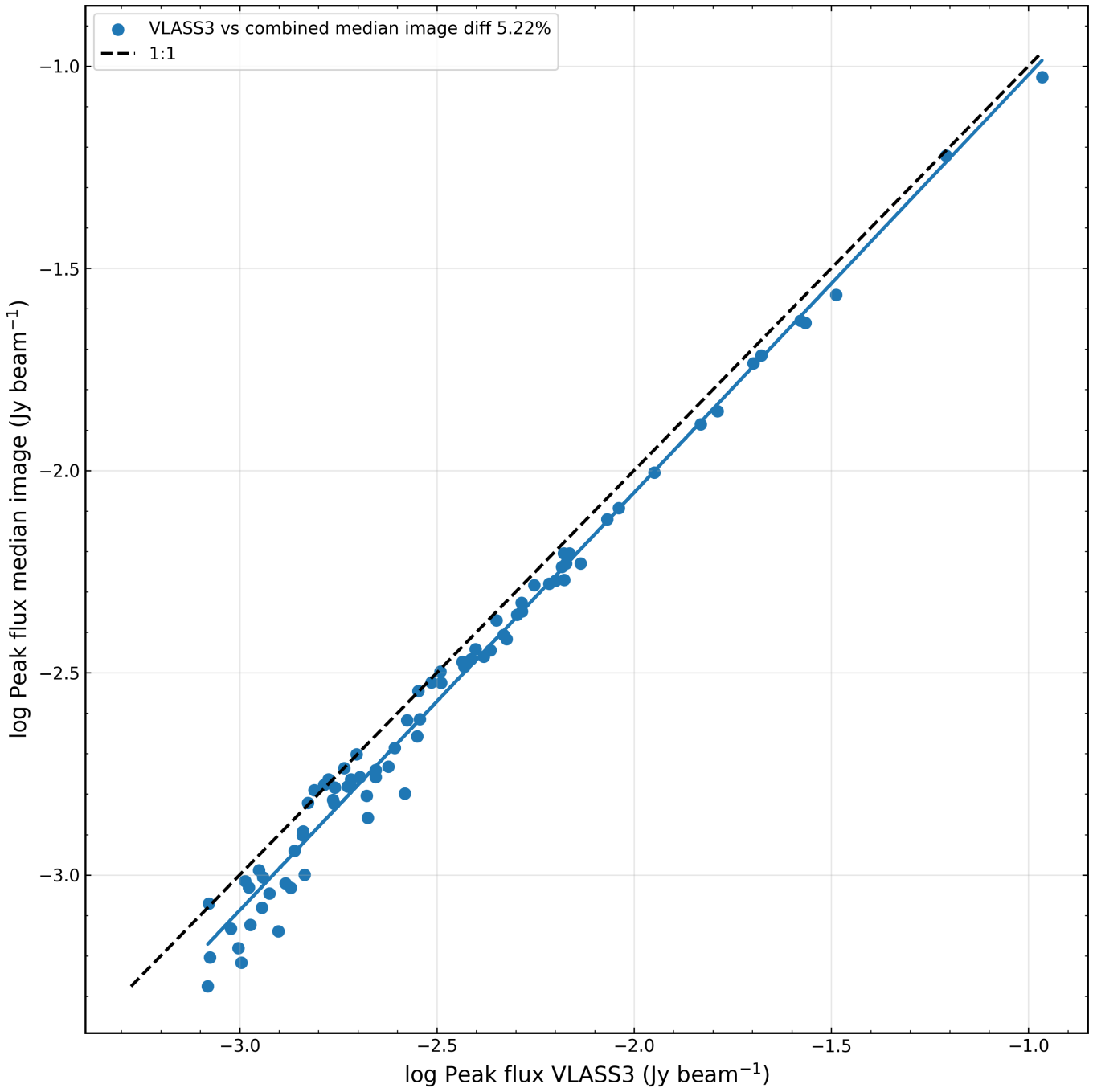

Figure 32: Peak flux densities comparisons between VLASS epoch 3 (QL) and combined median maps.

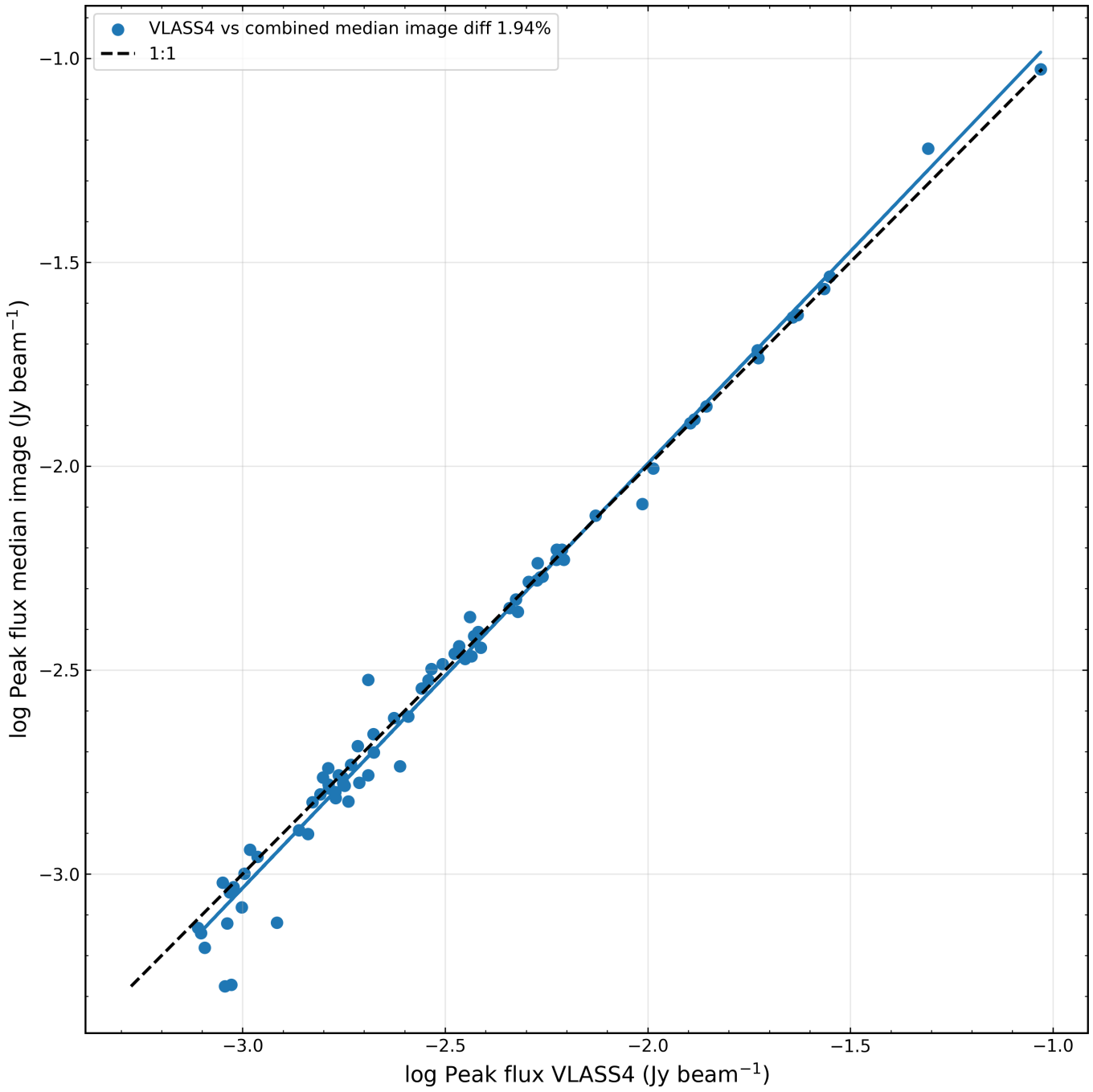

Figure 33: Peak flux comparisons between VLASS epoch 4 (QL) and combined median maps.

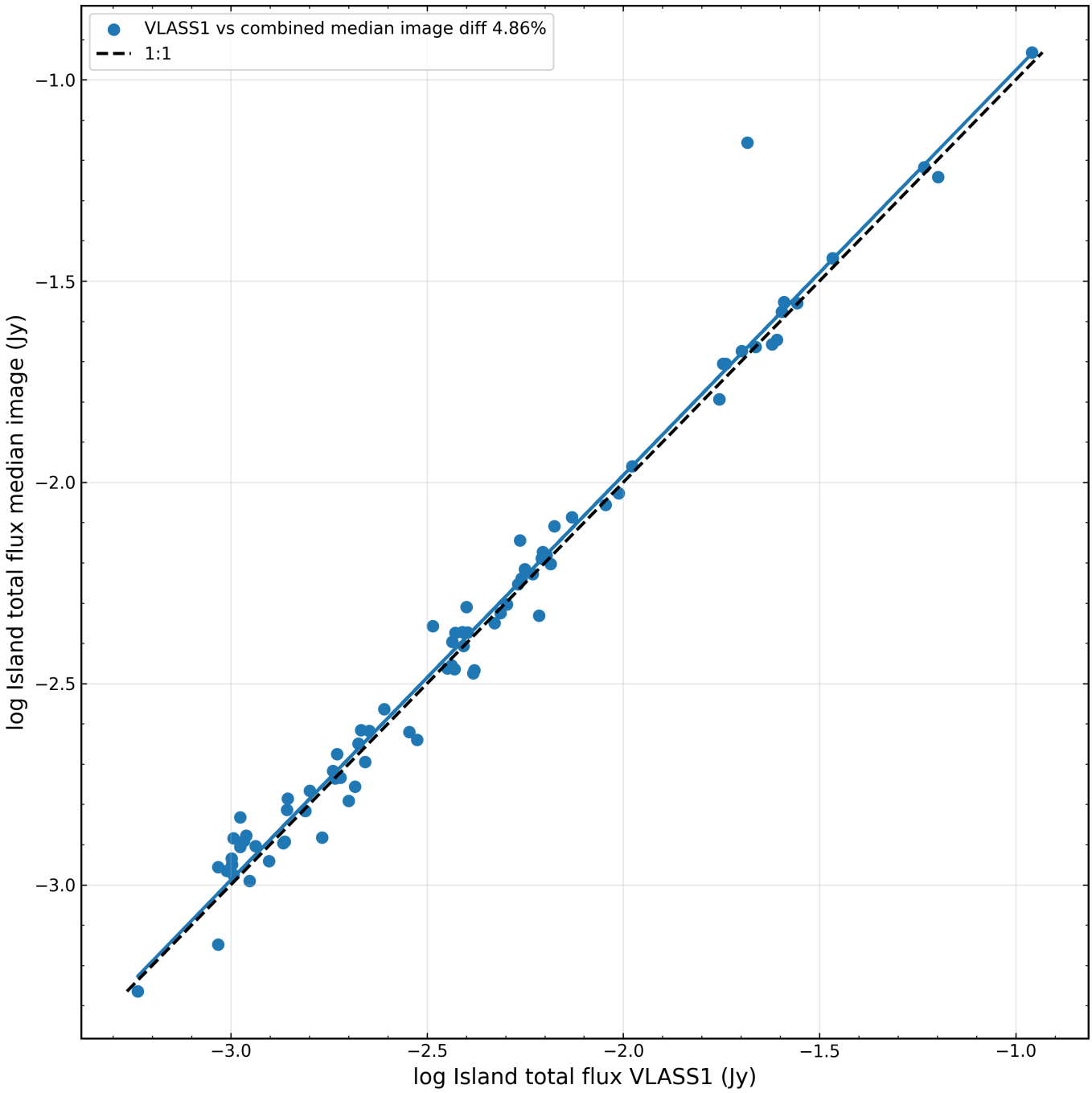

Figure 34: Island flux comparison between VLASS epoch 1 (QL) and combined median maps.

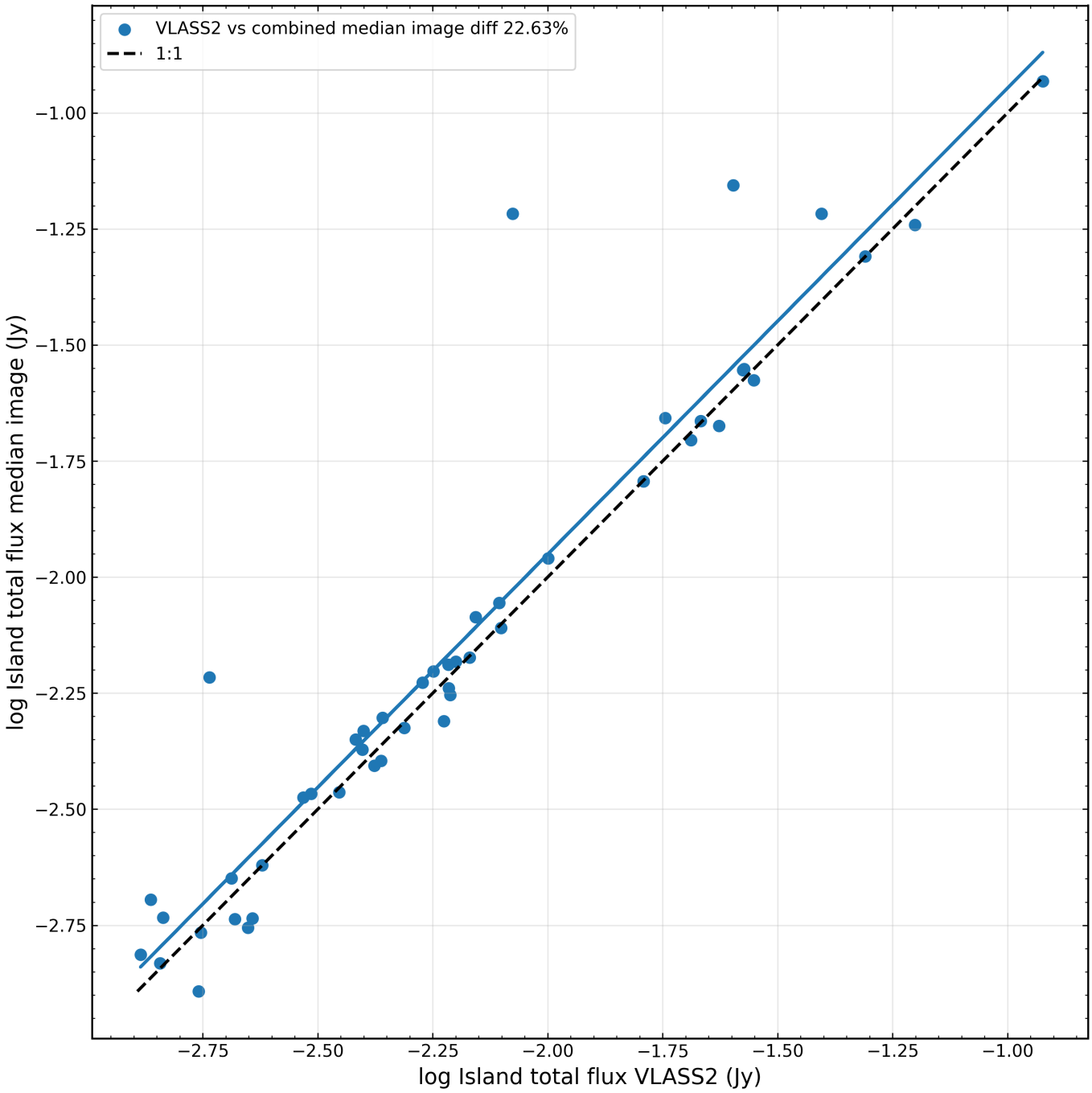

Figure 35: Island flux comparison between VLASS epoch 2 (QL) and combined median maps.

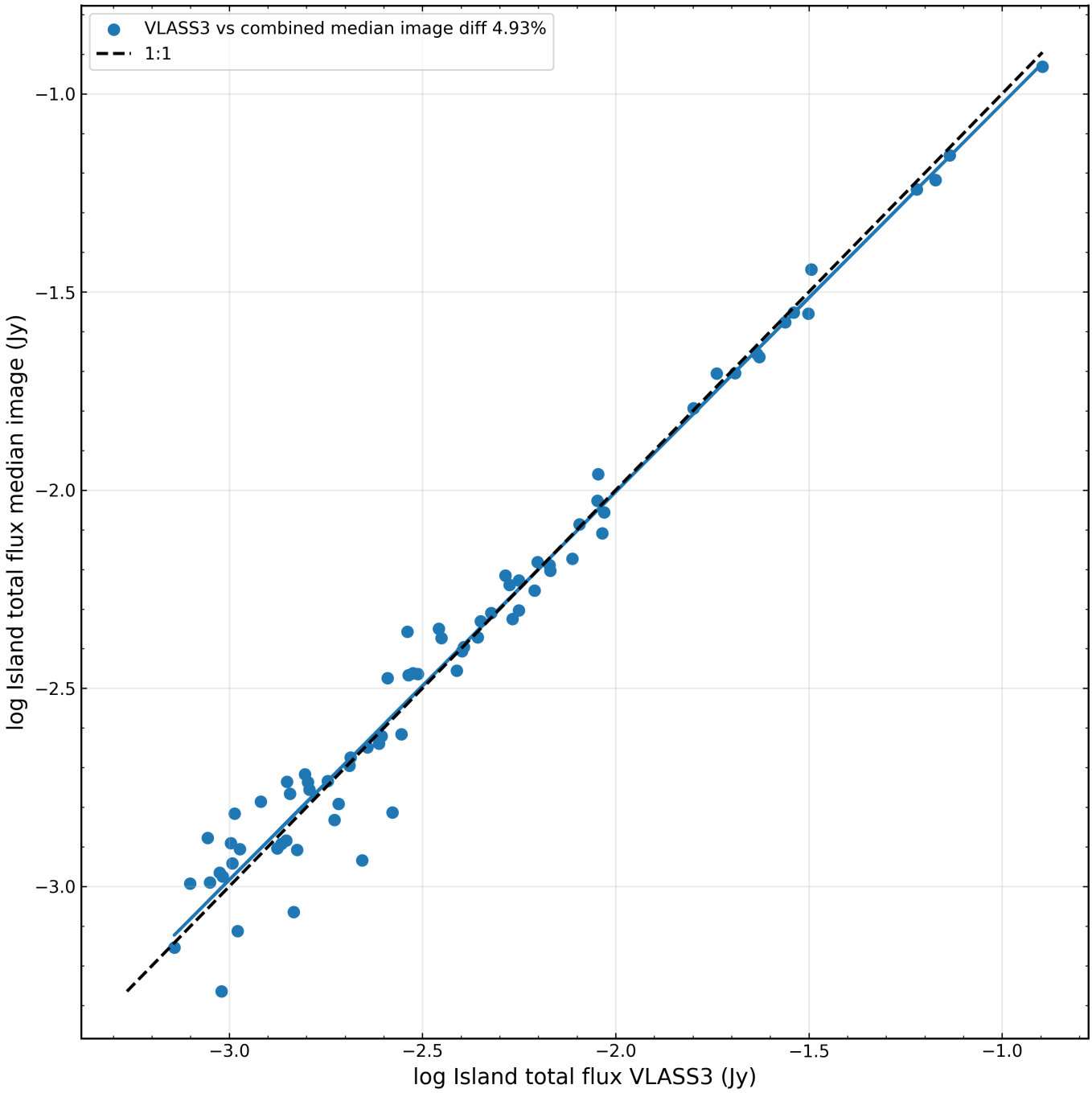

Figure 36: Island flux comparison between VLASS epoch 3 (QL) and combined median maps.

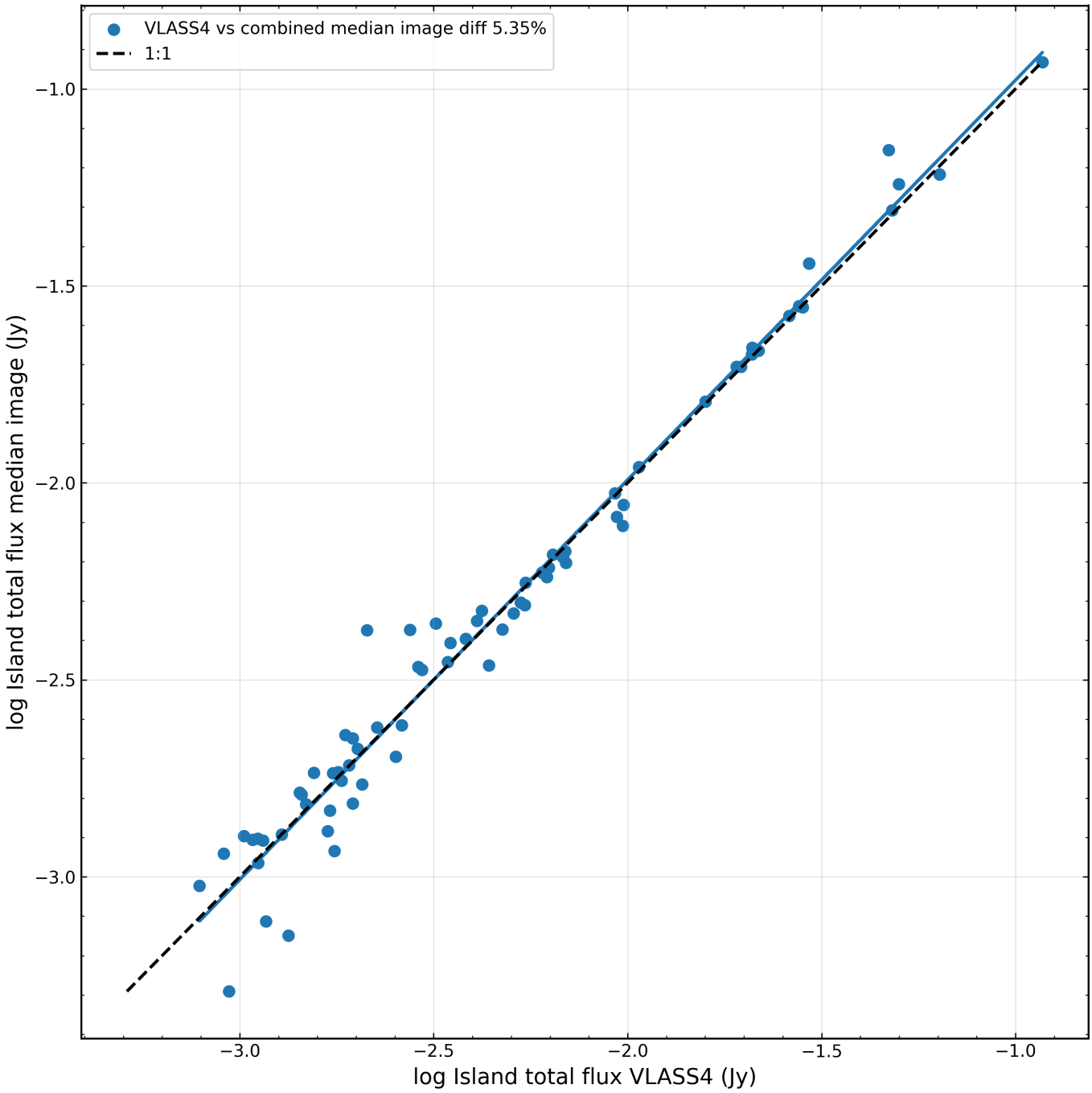

Figure 37: Island flux comparisons between VLASS epoch 4 (QL) and combined median maps.

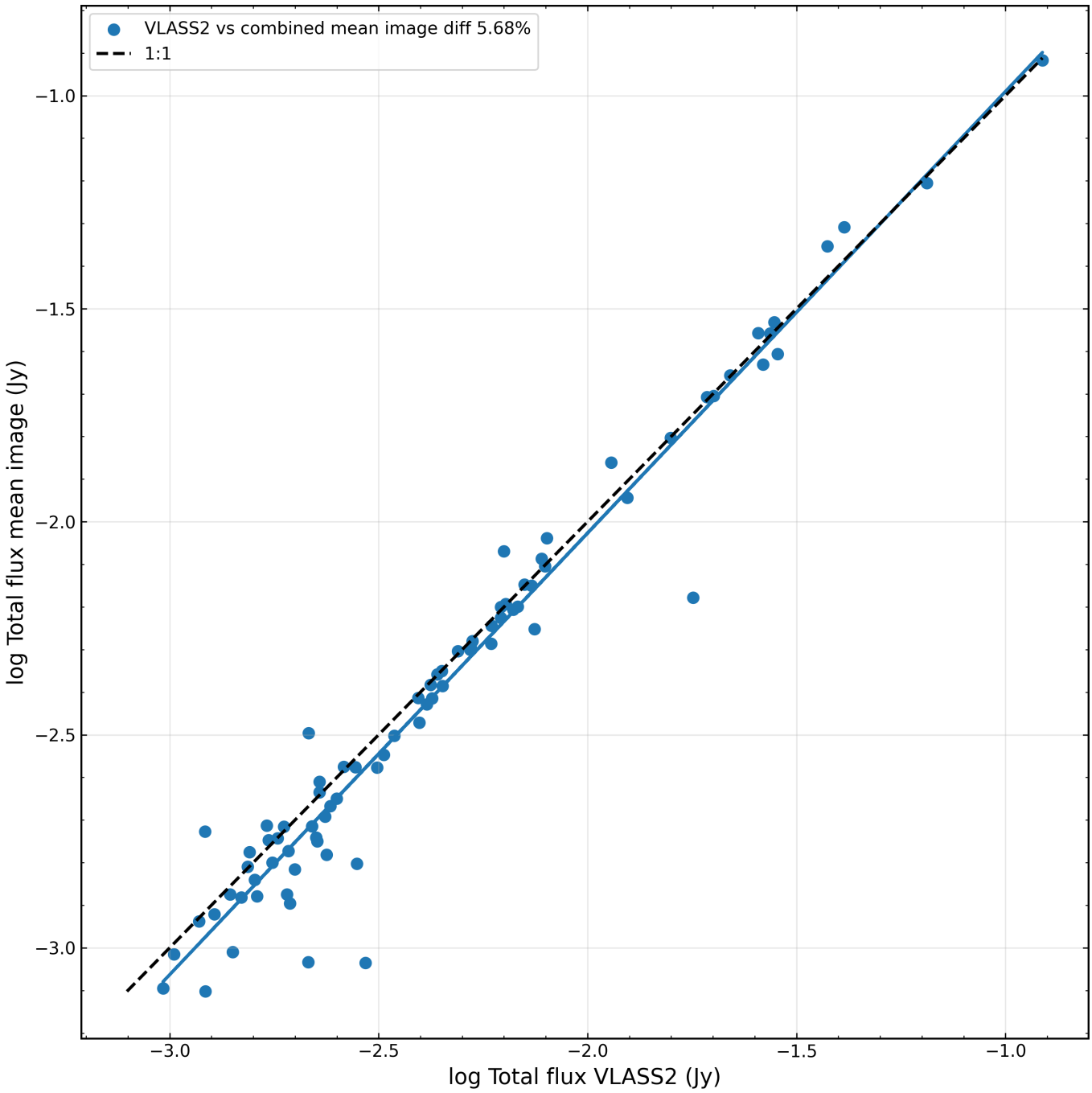

Figure 38: Flux densities comparisons between VLASS epoch 2 (SE) and combined mean maps.

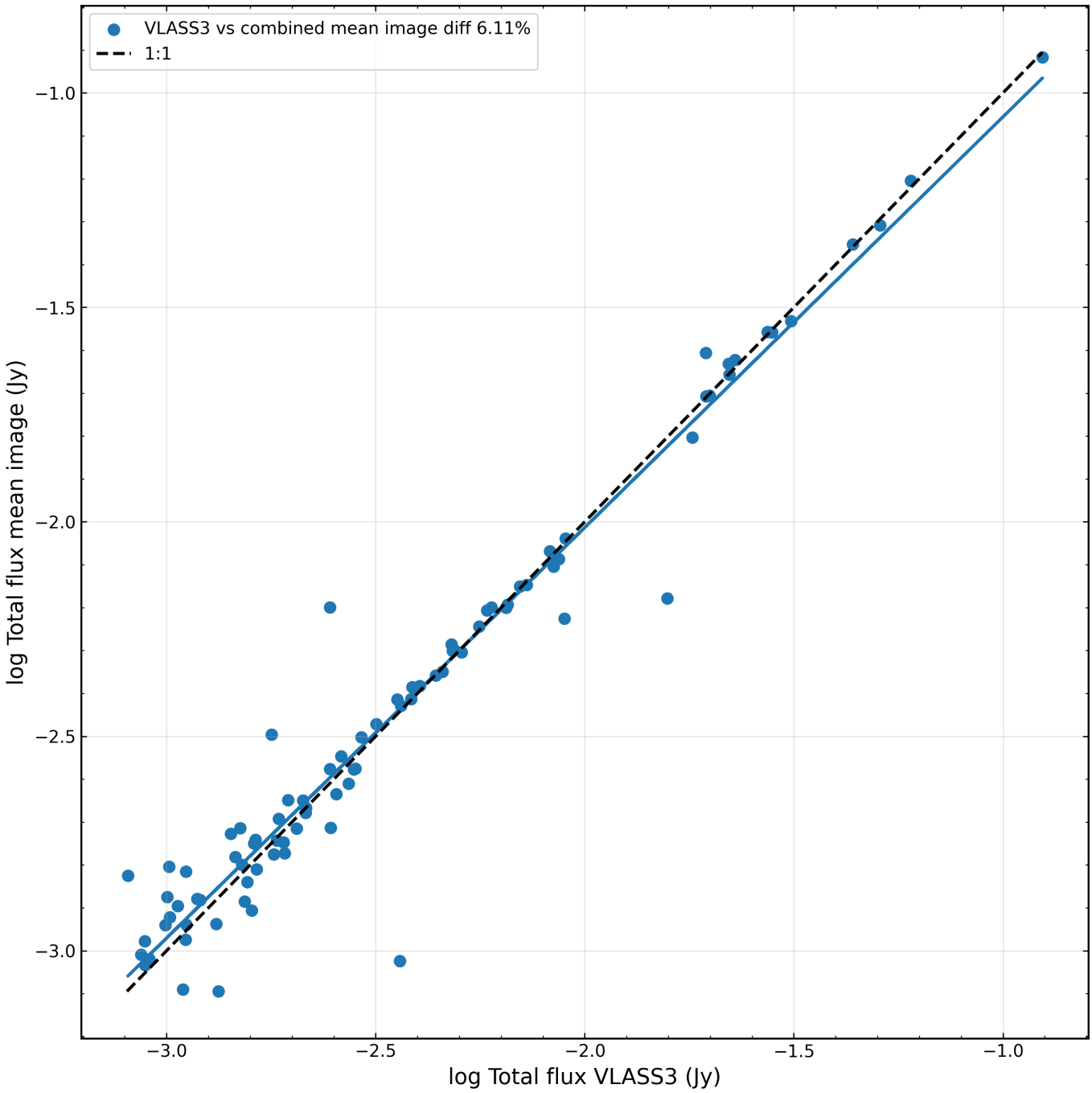

Figure 39: Flux densities comparisons between VLASS epoch 3 (SE) and combined mean maps.

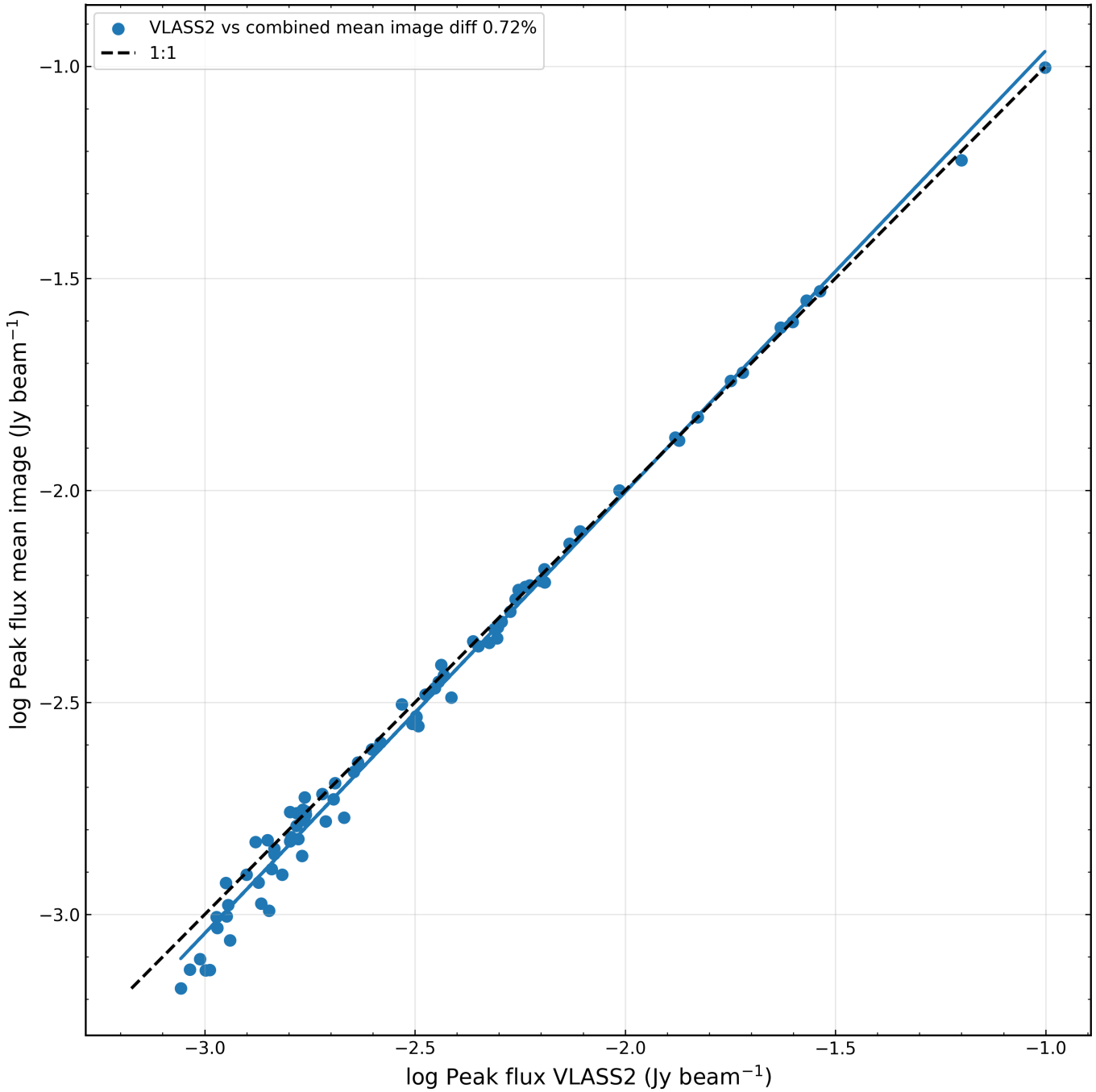

Figure 40: Peak flux comparisons between VLASS epoch 2 (SE) and combined mean maps.

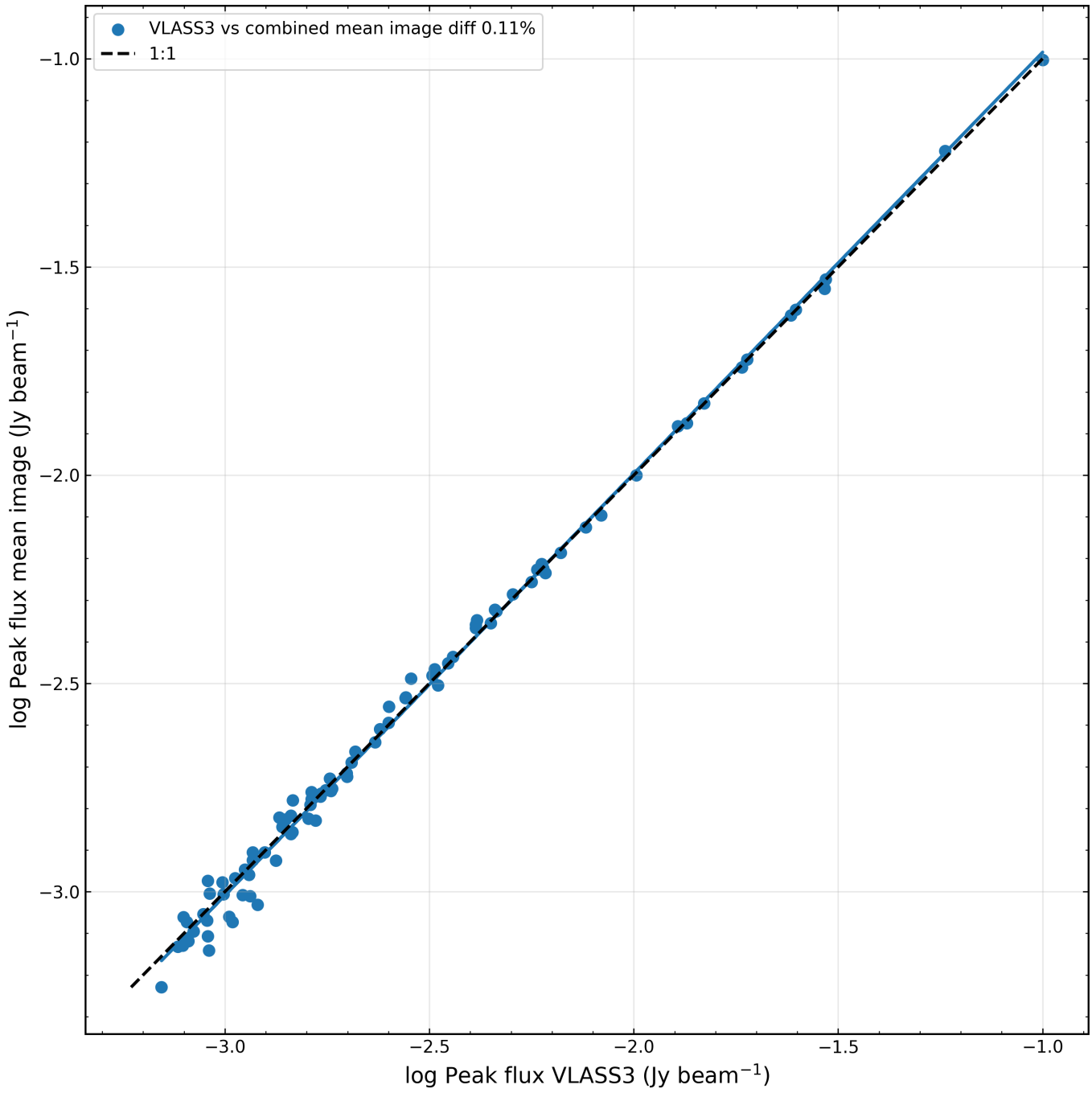

Figure 41: Peak flux densities comparisons between VLASS epoch 3 (SE) and combined mean maps.

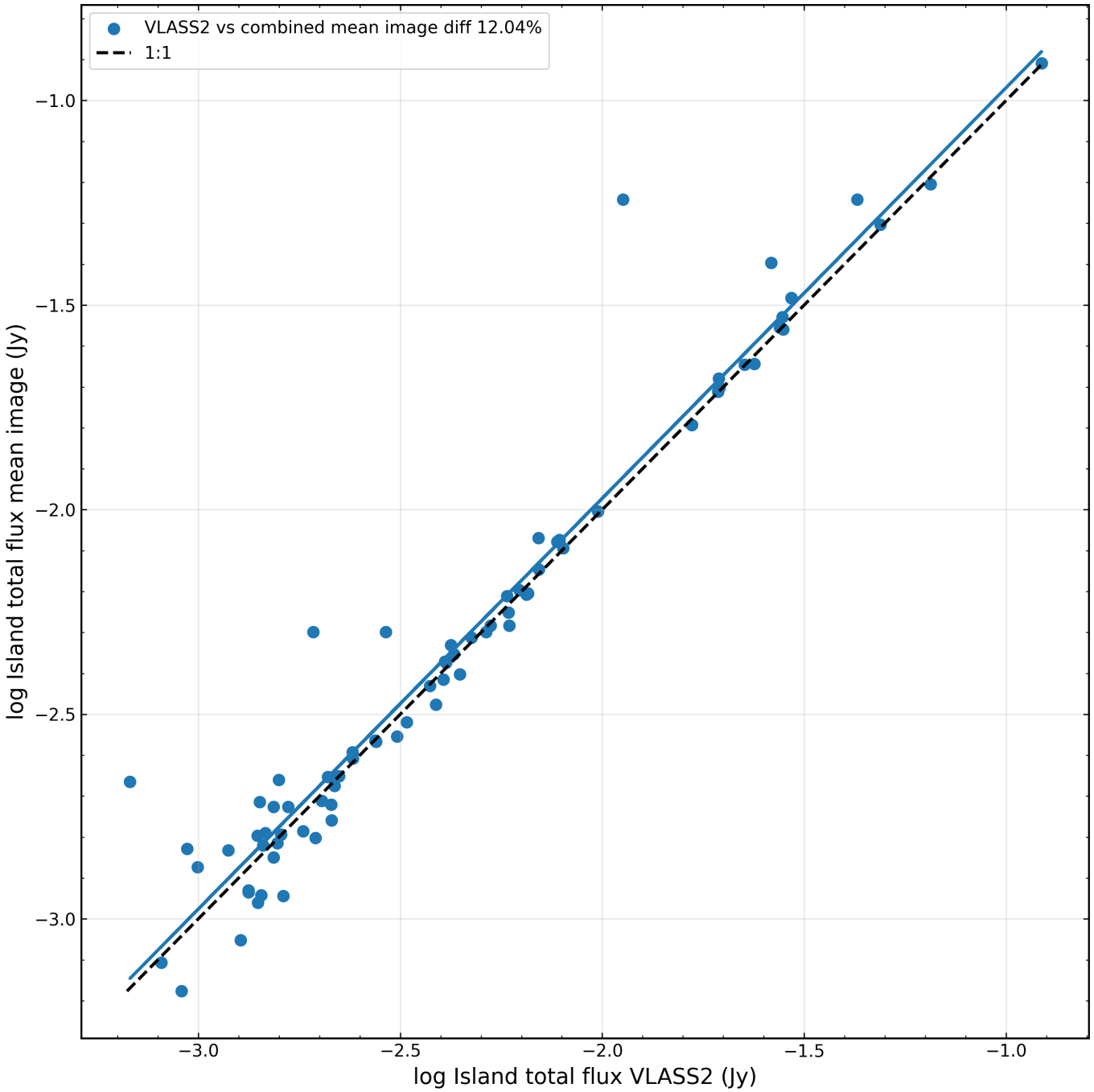

Figure 42: Island flux comparison between VLASS epoch 2 (SE) and combined mean maps.

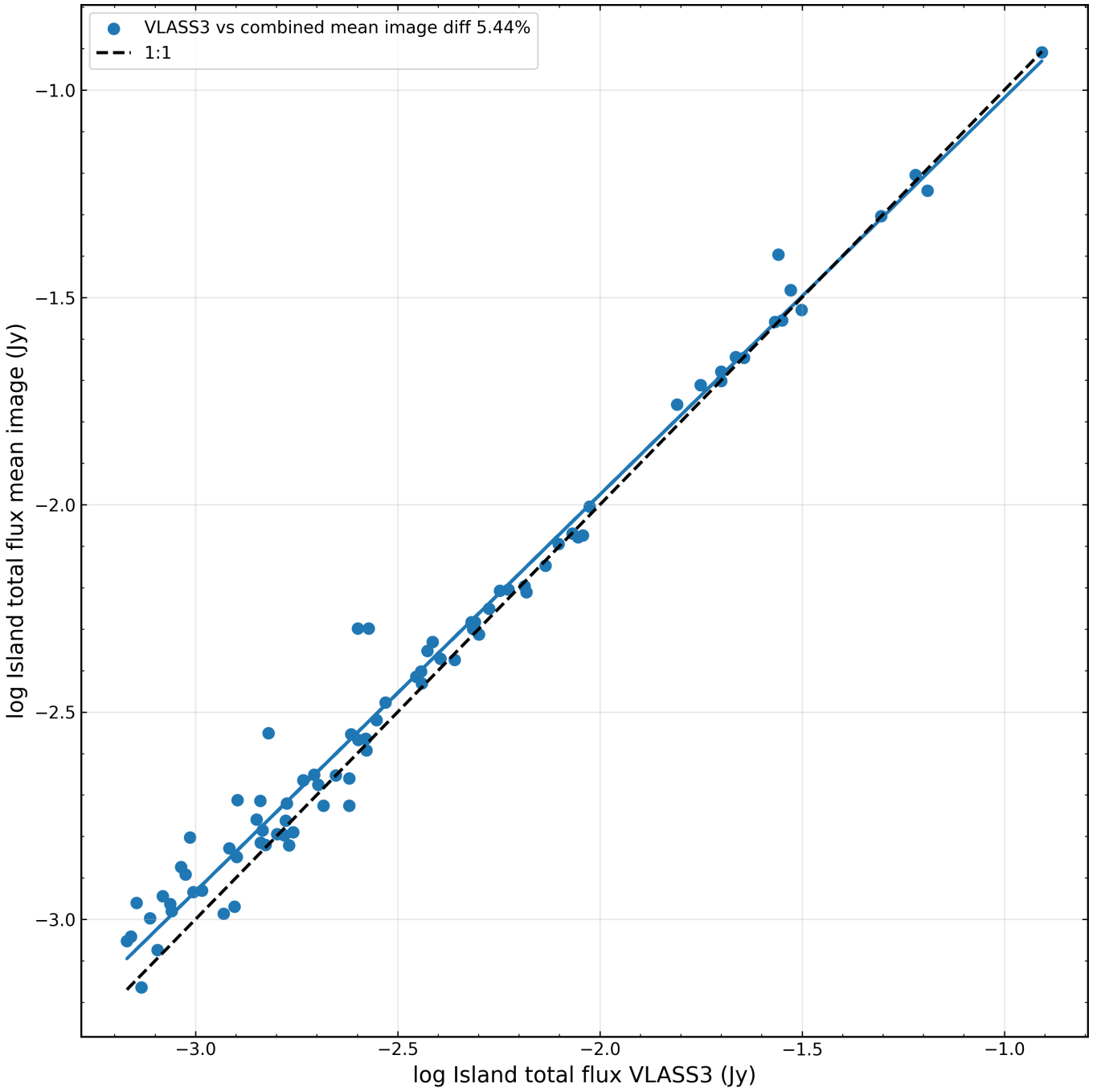

Figure 43: Island flux comparisons between VLASS epoch 3 (SE) and combined mean maps.

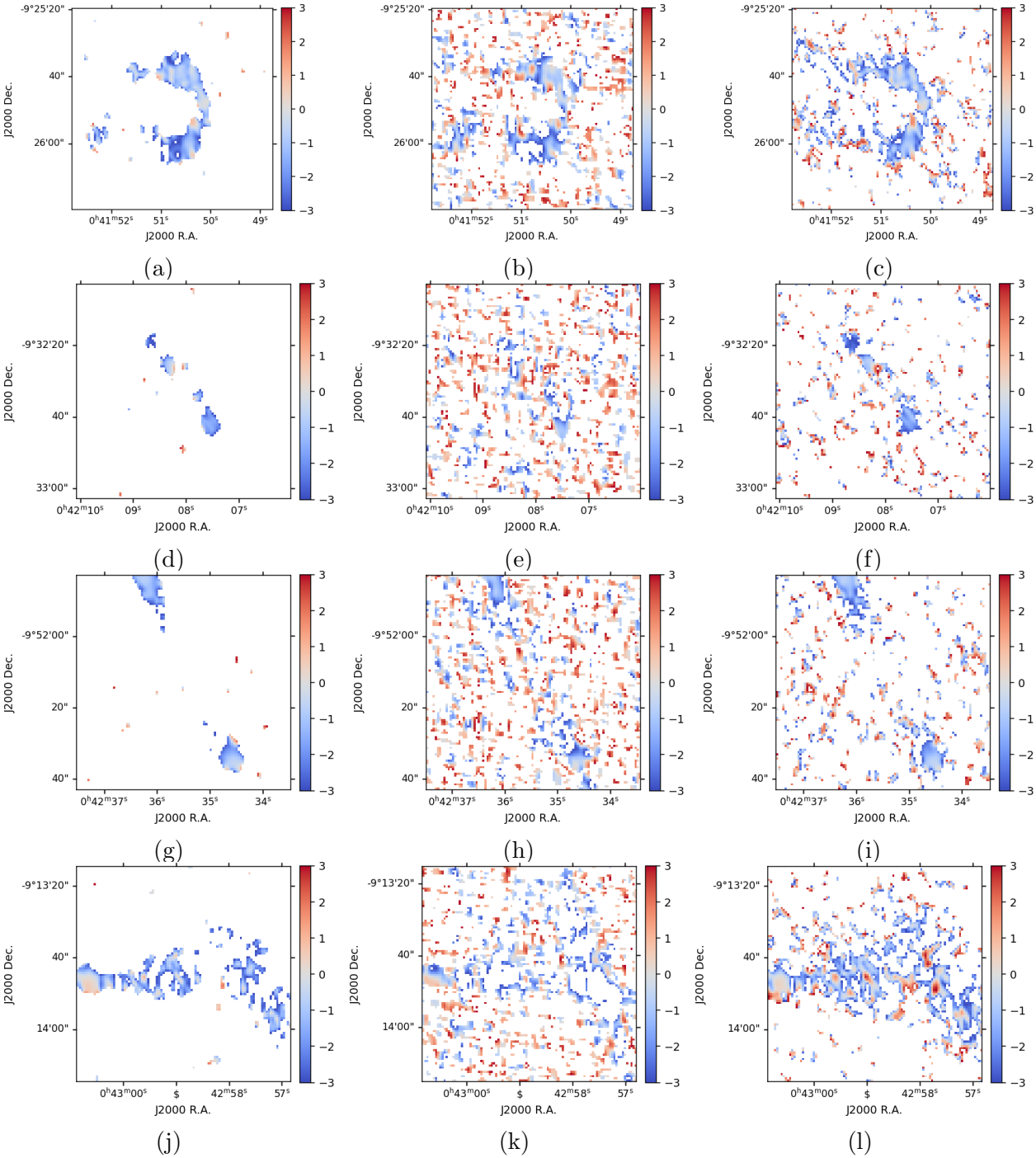

Figure 44: Cutouts of alpha (spectral index) maps. Combined alpha map compared with the individual VLASS epoch alpha map for the same SE data shown above. The first map from each row is a combined alpha map. The second map from each row is the VLASS2 alpha map. The third map from each row is the VLASS 3 alpha map. For comparison, we convolved each VLASS alpha map to a common beam of $3.23'' \times 2.27''$, $15.89°$.

Acknowledgment

VP acknowledges Mark Lacy for fruitful discussions on the VLASS image-combination work.

Appendix

A Uncertainty treatment for integrated, island, and peak flux density comparisons

To compare source flux densities measured from the VLASS single epoch and combined images, we cross-matched common PyBDSF detections within a $1''$ matching radius. For each matched source, both integrated flux density ($S_{\rm int}$) and peak flux density ($S_{\rm peak}$) were extracted from the PyBDSF source catalog.

For the integrated and island flux densities, the total uncertainty was computed by adding in quadrature two contributions: a fractional calibration term and an image-noise term scaled by the effective number of synthesized beams subtended by the source. The integrated-flux uncertainty for source i was taken as

$$\sigma_{{\rm int},i} = \left[(f_{\rm cal} S_{{\rm int},i})^2 + \left(\sigma_{{\rm rms},i} \sqrt{N_{{\rm beam},i}} \right)^2 \right]^{1/2}, \tag{1}$$

where $f_{\rm cal}$ is the adopted fractional calibration uncertainty, and $\sigma_{{\rm rms},i}$ is the local island RMS reported by PyBDSF. In this analysis, we adopted $f_{\rm cal} = 0.05$.

The number of synthesized beams covered by a source was estimated from the PyBDSF source size and the restoring beam size of the image:

$$N_{{\rm beam},i} = \frac{\theta_{{\rm maj},i}\, \theta_{{\rm min},i}}{\theta_{\rm bmaj}\, \theta_{\rm bmin}}, \tag{2}$$

where $\theta_{{\rm maj},i}$ and $\theta_{{\rm min},i}$ are the fitted major and minor axes of the source, and $\theta_{\rm bmaj}$ and $\theta_{\rm bmin}$ are the restoring beam major and minor axes from the FITS header. To avoid nonphysical values for unresolved sources, we imposed

$$N_{{\rm beam},i} \geq 1. \tag{3}$$

For the peak flux density, the total uncertainty was likewise computed in quadrature from a 5% calibration term, and the local RMS:

$$\sigma_{{\rm peak},i} = \left[(f_{\rm cal} S_{{\rm peak},i})^2 + \sigma_{{\rm rms},i}^2 \right]^{1/2}, \tag{4}$$

with the same adopted calibration fraction $f_{\rm cal} = 0.05$.

B Uncertainty on flux differences between images

For any two matched measurements S_a and S_b, the uncertainty on the flux difference was computed by quadrature addition:

$$\sigma_{\Delta S} = \left(\sigma_a^2 + \sigma_b^2 \right)^{1/2}, \tag{5}$$

where σ_a and σ_b are the total uncertainties for the two images being compared. This was applied separately for integrated flux density and peak flux density.

C Percentage differences after accounting for uncertainty

The percentage-difference calculation was modified to account for measurement uncertainty. First, the absolute difference between two matched measurements was calculated:

$$\Delta S = |S_a - S_b|. \tag{6}$$

The uncertainty on this difference, $\sigma_{\Delta S}$, was then subtracted to estimate the residual difference above the measurement uncertainty:

$$\Delta S_{\rm net} = \max\left(\Delta S - \sigma_{\Delta S},\, 0\right). \tag{7}$$

The percentage difference for each source was then defined relative to the reference flux S_a as

$$\delta(\%) = 100 \times \frac{\Delta S_{\rm net}}{S_a}. \tag{8}$$

Thus, the mean percentage difference reported for a given image pair was

$$\langle \delta(\%) \rangle = \left\langle 100 \times \frac{\max\left(|S_a - S_b| - \sqrt{\sigma_a^2 + \sigma_b^2},\, 0\right)}{S_a} \right\rangle. \tag{9}$$

In addition, the mean percentage uncertainty on the difference was computed as

$$\langle \delta_\sigma(\%) \rangle = \left\langle 100 \times \frac{\sqrt{\sigma_a^2 + \sigma_b^2}}{S_a} \right\rangle. \tag{10}$$

The same formulation was used for both integrated flux density and peak flux density comparisons, and for both mean- and median-based analyses.

D Flux ratios and robust summary statistics

In addition to percentage differences, the matched-source comparisons were summarized using the flux-density ratio

$$R = \frac{S_b}{S_a}, \tag{11}$$

$$\text{median ratio} = \text{median}(R), \tag{12}$$

and the median absolute deviation (MAD),

$$\text{MAD} = \text{median}\left(|R - \text{median}(R)|\right). \tag{13}$$

E Statistics for QL maps

Table 5: Matched-source comparison statistics for the VLASS QL maps (Fig. 5) relative to the weighted mean and weighted median combined maps. For each flux measure, the entries are listed as median ratio / MAD / mean % diff.

Epoch	Total flux		Peak flux		Island total flux	
	Mean map	Median map	Mean map	Median map	Mean map	Median map
VLASS1	0.95 / 0.11 / 10.77	0.97 / 0.09 / 8.42	1.06 / 0.08 / 2.65	1.03 / 0.06 / 2.15	1.04 / 0.07 / 8.18	1.05 / 0.07 / 4.86
VLASS2	0.93 / 0.11 / 9.33	0.95 / 0.11 / 8.40	0.97 / 0.05 / 1.06	0.95 / 0.04 / 1.12	1.07 / 0.09 / 27.50	1.03 / 0.09 / 22.63
VLASS3	0.95 / 0.08 / 6.61	0.96 / 0.08 / 6.18	0.89 / 0.05 / 3.91	0.87 / 0.04 / 5.22	1.02 / 0.11 / 4.85	1.00 / 0.11 / 4.93
VLASS4	0.98 / 0.09 / 6.67	0.99 / 0.07 / 6.72	1.02 / 0.08 / 1.91	1.00 / 0.05 / 1.94	1.02 / 0.10 / 4.21	1.01 / 0.09 / 5.35

F Statistics for SE maps

Table 6: Matched-source comparison statistics for the VLASS SE maps (Fig. 6) relative to the weighted mean combined map. For each flux measure, the entries are listed as median ratio / MAD / mean % diff.

Epoch	Total flux	Peak flux	Island total flux
VLASS2	0.96 / 0.07 / 5.68	0.97 / 0.05 / 0.72	1.01 / 0.06 / 12.04
VLASS3	1.02 / 0.07 / 6.11	1.00 / 0.04 / 0.11	1.06 / 0.08 / 5.44